UCLouvain

epl

École polytechnique de Louvain

Tracking Asian hornets with low power harmonic radars : applicative constraints and tag design

Author: **Pei-Hao Ye**
Supervisors: **David Bol, Dimitri Lederer**
Readers: **Christophe Craeye, Marco Gonzalez, Pol Maistriaux**
Academic year 2023–2024
Master [120] in Electrical Engineering

Abstract

The Asian hornet, an invasive species originating from Southeast Asia, has recently become widespread in Southern Europe. Due to its rapid spread and the serious threat it poses to local honeybee colonies, various solutions and technologies are currently under investigation. This paper consolidates most of these approaches to provide a comprehensive overview of the available options. We evaluate the pros and cons of each method to determine the most suitable one for our application. We then outline a method for defining the system parameters and predicting its performance, specifically focusing on the detection range, which is determined to be 12 meters with an EIRP of 40 dBm. Next, we focus on improving performance by optimizing the tag. A model and methodology are described to achieve this goal, potentially extending the detection range to 18 meters. Finally, an antenna experiment is conducted to validate the simulation results. This work offers a general overview of the Asian hornet problem, describes potential technologies for controlling the spread of this species, and presents a real-time functioning tag design.

Contents

List of Tables

List of Figures

Chapter 1

Introduction

Context

Scientists, farmers, and environmentalists are increasingly alarmed by the presence of Asian hornets (Vespa velutina) in Europe. These invasive predators, originally from Southeast Asia, were accidentally introduced to Europe in the early 2000s[14]. Their rapid spread poses a significant threat to local biodiversity and fragile ecosystems, potentially leading to a serious decline in honey production and compromised crop pollination. This is because Asian hornets, often called "bee-killers," pose a grave danger to bee colonies[15]. The lack of natural predators for the Asian hornet in Europe is particularly concerning, as it facilitates their unchecked proliferation and amplifies their harmful effects on native fauna[23]. The spread of Asian hornets represents a significant ecological challenge that requires urgent action to mitigate their impact on bee populations and ecosystem resilience. Developing sustainable strategies to protect bee populations and preserve the delicate balance of our natural environment is essential to address this issue[25].

Contribution

Current research on the tracking of Asian hornets typically discusses only up to three methods [16], which is relatively limited given the complexity and significance of the issue. The primary contribution of this work lies in consolidating and presenting the various existing technologies related to tracking Asian hornets and monitoring insects. This includes both the technologies currently available on the market and those still in development. By doing so, this work provides a comprehensive overview of the possibilities, enabling the selection of the most appropriate technology for our specific application based on clearly defined criteria.

Another significant contribution is the determination of the system parameters, ensuring compliance with national standards. The work meticulously details the entire process from selecting the technology to defining the parameters and finally predicting the system's performance in terms of detection distance. This comprehensive approach goes beyond what is typically presented in the literature, which often addresses only parts of this process.

Finally, the work contributes by optimizing a key part of the system to achieve better performance through simulations. The research does not stop at theoretical analysis, it also includes experimental validation to verify the simulation results.

Structure

Chapter 2 provides general information on the Asian hornet, including its life-cycle and diet, followed by a presentation of various existing technologies related to the hornet problem, as well as insect monitoring technologies available on the market or still under development.

Chapter 3 covers the basic concepts of radar systems in general, studies the state of the art of harmonic radars, and provides system parameters based on all relevant constraints.

Chapter 4 deals with the design of a harmonic tag, from the selection of the diode to its configuration in practice. The methodology for worst-case design is also described in this chapter.

Chapter 5 presents the experiment results of the developed tag, along with a clear explanation of the experimental setup.

Chapter 6 summarizes this work, highlighting the key steps in each chapter.

Chapter 2

Context

As the main subject of this topic is around Asian hornet, a more in-depth knowledge is required to better understand its characteristics and behaviors.

This section first provide a comprehensive overview of hornets, including an in-depth analysis of their ecological impact and seasonal behavior. This is followed by a more detailed examination of these impacts and their broader implications. Subsequently, the section explores various existing methods, both those specifically designed for hornet management and those with broader applications, discussing their respective advantages and disadvantages.

2.1 Information on Asian Hornet

Vespa velutina, commonly known as the Asian hornet, is an insect belonging to the Hymenoptera order, native to southern Asia. Although primarily found in these regions, its presence has been rapidly expanding across Europe in recent years [42].

Asian hornets, like other hornet species, construct nests and exhibit highly developed hunting skills. These insects can be classified into two primary categories, similar to the system observed in bees: workers and queens. The queens, being larger in size, are primarily responsible for reproduction within the colony. In contrast, the workers, which are smaller and non-reproductive, play a crucial role in maintaining the daily operations of the colony. Their tasks include foraging for food, caring for the young and expanding the nest. This division of labor ensures the colony's continued growth and survival throughout the year [42].

Seasonal Activity Pattern

As the Chinese proverb suggests, "If you know the enemy and know yourself, you can win a hundred battles" it is essential to thoroughly understand the Asian hornet's life cycle to devise effective control strategies. Their annual activities are summarized in Fig. 2.1.

The life cycle begins in spring, when the queens emerge from hibernation and seek suitable locations to establish nests, typically in sheltered areas such as tree cavities, hedges or building eaves. Each queen usually works independently, building

her nest alone. Once the initial nest is finished, the queen lays eggs and rears the first generation of workers. As the colony grows, the population reaches the nest's maximum capacity, typically around 100 individuals. At this point, the colony constructs a larger secondary nest nearby, which will house the colony through the winter and can eventually host up to 6 000 hornets [38, 45].

With the onset of summer, the hornet population peaks, and the demand for protein sources is at its highest. A single hornet can hunt up to 50 insects daily, making this period when they have the most significant impact on surrounding ecosystems [38, 45].

In autumn, the colony focuses on the fertilization of new queens, which will survive to start the next life cycle. Typically, between 180 and 500 new queens are produced per nest [38, 45].

Finally, in winter, the new queens leave the nest to hibernate, while the workers gradually perish as temperatures drop [38, 45].

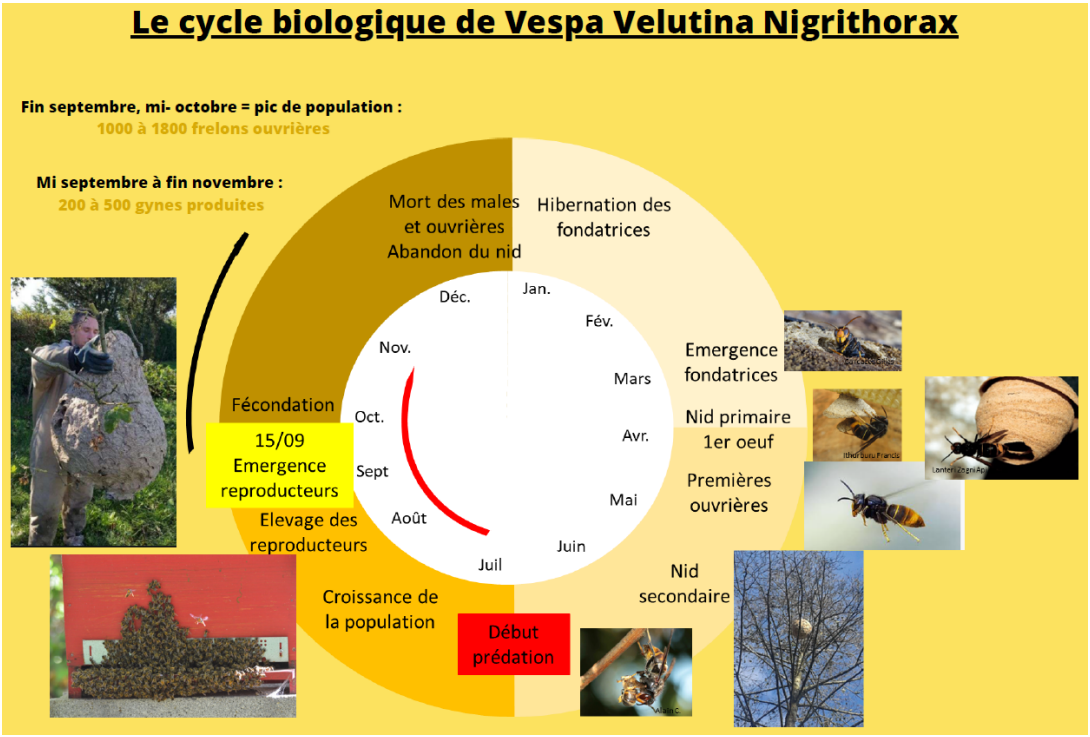

Figure 2.1: Lifecycle of Asian hornet from [9]

Diet & Threats

The rapid spread of Vespa velutina across Europe can be attributed to several factors. Now, let's delve into the dietary habits of these hornets. Asian hornet workers rely on two primary nutrient sources: nectar collection and predation. When hunting, workers capture prey, retaining only the thorax, which is rich in protein, to bring back to the nest. This protein-rich thorax is fed to the larvae, which in turn, regurgitate a nutrient-rich substance containing proteins and sugars. This substance becomes the primary food source for adult workers [31].

Research from [29] has shown that while the diet of Asian hornets varies across different environments, a consistent trend is observed: bees and bumblebees constitute approximately 40% of their diet, as illustrated in Fig. 2.2.

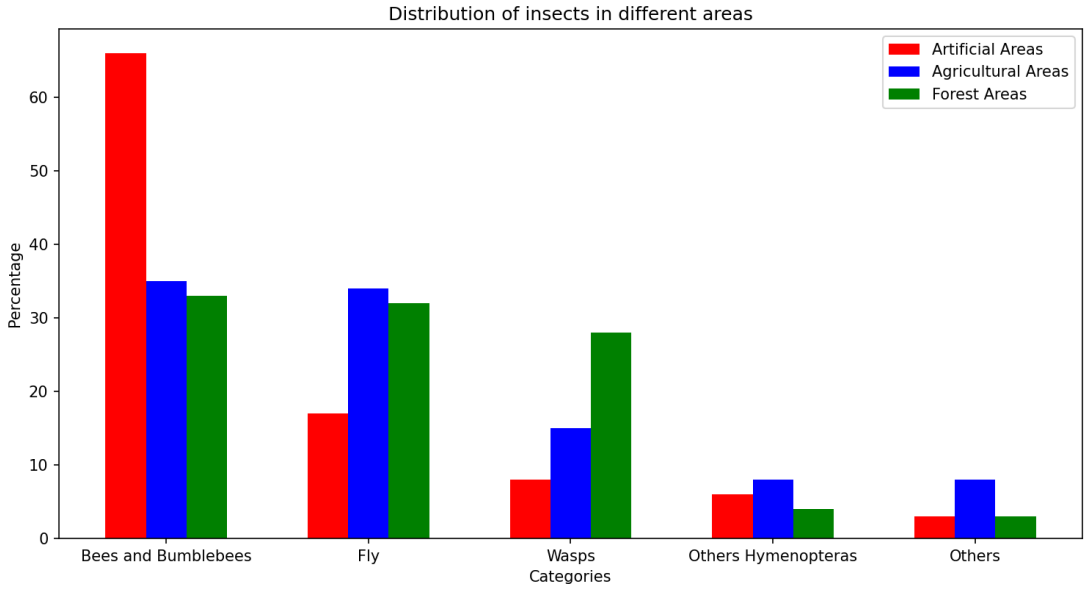

Figure 2.2: Diet of Asian hornet in different environements

Based on this data, the total mass of insects consumed by hornet nests of varying sizes has been calculated. For instance, an average-sized nest consumes about 11.32 kg of insects annually. Given the average size and mass of a bee, it is estimated that each nest is responsible for the predation of around 5 000 bees, significantly contributing to the decline in bee populations. This alarming impact underscores the urgent need for effective protection measures [31].

2.2 Techonology

This section explores various methods developed over recent decades to address this issue. These methods can be broadly categorized into two approaches: protecting beehives and locating hornet nests. For each method, we examine the characteristics, advantages and disadvantages in detail.

Insect trap

One of the earliest techniques employed to control the Asian hornet is the use of insect traps. These traps are designed to lure the target insect into a device from which it is impossible to escape. Traps can be categorized into two types: selective and non-selective. Selective traps are designed to capture only hornets, allowing other insects to escape, while non-selective traps capture all insects indiscriminately [1].

A common example of a non-selective trap is a beer trap, which can be easily assembled at home, as illustrated in Fig. 2.3. The process involves placing the trap in a strategic location for a set period and monitoring the captured insects. However,

the selectivity rate for such traps is extremely low, at only 0.55%, which is problematic as it inadvertently affects non-target species, thereby disrupting ecosystems [1].

Figure 2.3: Example of non-selective bait trap from [17]

More sophisticated options, such as the "Jade Prode" selective trap, are available on the market. This trap is specifically designed for Asian hornets, featuring access points calibrated to within a hundredth of a millimeter. This precision allows smaller insects such as bees, wasps and flies to escape through the openings, while preventing larger insects, like the European hornet queen, from entering, as shown in Fig. 2.4. Priced at 55€, this trap is relatively affordable and reusable, although its long-term effectiveness remains uncertain [26].

Figure 2.4: Selective Bait trap from Jade Prode [26]

Muzzle

As previously mentioned, hornets consistently target bees, particularly around hive entrances where they position themselves to capture foraging bees with ease. The presence of hornets creates a constant buzzing sound that agitates the bees, often causing them to remain inside the hive, which disrupts the colony's food intake

and must be avoided [34].

A second method for mitigating hornet attacks involves the use of a hive muzzle designed to protect hive entrances from predators and intruders, as shown in Fig. 2.5. While the muzzle shields bees from direct attacks when they are inside the hive, it does not offer protection once the bees leave in search of pollen. However, the presence of this protective device appears to embolden the bees, making them more likely to venture out for foraging, even when hornets are nearby [34].

Figure 2.5: Example of muzzle from [34]

Strategy change

Despite the benefits of these protective measures, their effectiveness diminishes as the hornet population continues to grow. To address this, a shift in strategy is required, moving from protecting the bees to directly targeting and eliminating hornets at their nests. This approach aims to slow down the reproduction of worker hornets and reduce their numbers in the area. Although not a permanent solution, it is effective in limiting the damage caused by these predators. New techniques have emerged to locate hornet nests, which can be broadly classified into two methods: tracking hornets or conducting ground searches.

Table of criteria

Before discussing the various technologies, it is important to establish the criteria guiding our selection. The current objective is to identify a solution that is cost-effective, rapidly deployable and highly reliable. We outline these criteria in detail below and systematically apply them to each of the technologies under consideration.

Number	Criteria	Description
1	Low cost	Is the entire equipment affordable?
2	Reliability	Does the process yield minimal false positives ?
3	Environnemental resistance	[/]
4	Maximum Range	[/]
5	Single time	Can the goal be achieved without repeating the process?
6	Weight of tag	[/]

Table 2.1: List of criteria

Infrared image

A novel method has recently been developed to address the challenge of locating hornet nests using thermal imaging technology. This approach uses infrared cameras to distinguish insects from their surroundings, as detailed in the document [32].

The method employs two types of cameras—infrared and standard—each capturing data that is processed through Convolutional Neural Networks (CNN) to extract relevant features. An Ensemble Learning algorithm is then applied to the combined output from the CNNs, generating an image that indicates the presence or absence of hornet nests [32]. However, to make this technology efficient, the captured images must include the nests. Consequently, the system requires mobility to survey the environment, which is why a drone is incorporated into the design, as depicted in Fig. 2.6 .

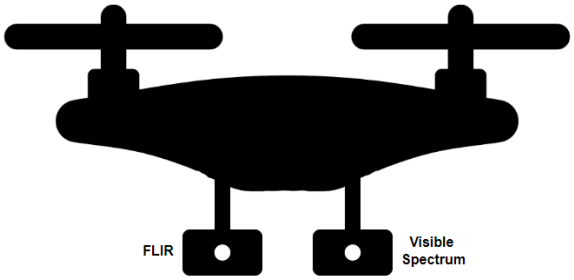

Figure 2.6: Schematic of the prototype

To evaluate the system's performance, two datasets were acquired using the drone, each corresponding to one of the cameras. The results were highly promising: out of 200 datasets containing hornet nests, the model accurately identified 186 (True Positives) with only 6 False Positives, achieving an accuracy of 97% and a recall of 93%.

A significant advantage of this technology lies in its ability to detect hidden nests using dual cameras. As illustrated in Fig. 2.7, the nest in the first image blends into its surroundings, making it difficult to identify. In contrast, using both infrared and standard cameras enhances the visibility of obscured nests, significantly improving detection accuracy [32] .

Figure 2.7: Example of positive infrared images by FLIR camera from [32]

Although not explicitly stated in the document, the ideal application would involve organizing drone patrols to systematically monitor the area. This technique shows considerable promise, effectively detecting hornet nests, whether exposed on the surface or concealed within trees.

	1	2	3	4	5	6
criteria	★☆☆	★★★	★★☆	N/A	×	N/A

Table 2.2: Criteria-based evaluation of thermal imaging

RFID

Another method worth mentioning within this category, due to its widespread use in observing insect colonies, is RFID (Radio Frequency Identification) technology. This technology is already prevalent in the commercial sector, particularly for purposes like theft prevention and inventory management.

RFID systems consist of two main components: an antenna and a tag. The tag is passive and typically small. When in proximity to the antenna, the tag is powered via magnetic coupling and transmits information back to the antenna. This information can then be analyzed for various purposes, such as identification [44].

Key characteristics of this technology include the tag's small size, lightweight design, and relatively limited detection range. The tag's miniaturized form makes it ideal for attaching to insects without disrupting their natural behavior. For instance, a study [36] demonstrated an RFID prototype designed to monitor bee activity. The tags used were 2.5 x 2.5 x 0.4 mm in size and weighed just 24 mg and is shown in the Fig. 2.8.

However, a significant challenge with this technology is its limited detection range. Addressing this issue would either require a redesign of the entire system or the deployment of numerous antennas to cover a larger area, both of which involve substantial resource commitments.

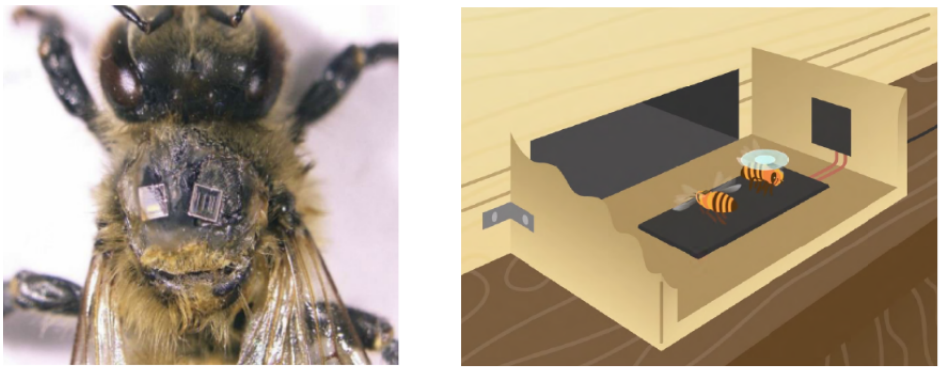

a) b)

Figure 2.8: RFID technology. (a) Bee equipped with tag from [16] (b) Principle schematic from [36]

	1	2	3	4	5	6
criteria	★★★	★★★	N/A	$\leq$ 0.5m	✓	N/A

Table 2.3: Criteria-based evaluation of RFID

Triangularisation

An alternative strategy for locating an Asian hornet nest involves tracking an individual hornet using a simple method known as the "wick pot" technique [40].

This approach does not rely on advanced technology and is based on calculating the time that is needed by the hornet to fly from a bait site to its nest and back. By determining this round-trip flight time, the distance to the nest can be estimated. The process is then repeated, progressively moving in the direction of the hornet's flight until the nest is located [40].

The methodology consists of the following steps:

1. Capture the hornet using a bait and induce temporary dormancy by cooling it.
2. Mark the hornet with a non-harmful color marker to distinguish it from others.
3. Release the hornet and observe its flight direction.
4. Record the hornet's round-trip flight time to estimate the distance to the nest.
5. Move closer to the nest in the indicated direction and repeat the procedure until the nest is found.

To made this methodology effective, several assumptions must be made:

- The hornet flies in a straight trajectory.
- A margin of error is considered, accounting for obstacle avoidance.
- The hornet does not switch from feeding stations.

Figure 2.9: Method application and target tracking trajectory from [40]

- There is only one nest within the search area.

The Fig 2.9 illustrates an example of the path followed. It is clear that this technique is time-consuming, as the process must be repeated multiple times. However, certain tricks can be employed to expedite the process, such as conducting repeated attempts in different locations to significantly narrow down the search area. The main advantage of this technique is its low cost, as it requires only basic equipment like a stopwatch and a marker. Additionally, it can accurately pinpoint the nest's location. The primary drawback, however, is the technique's reduced reliability when two nests are in close proximity. Moreover, the time required to determine the exact nest location is substantial, highlighting the need for a more efficient solution [40].

	1	2	3	4	5	6
criteria	★★★	★★☆	★☆☆	$\leq$ 500m	×	N/A

Table 2.4: Criteria-based evaluation of triangularisation

Retroflective-tag

A recent development in tracking hornets involves the use of retro-reflective tags combined with drone technology. This method, pioneered in 2021, utilizes everyday devices like UAVs equipped with cameras and light sources to track bees or hornets. The term "retro-reflective" refers to the property of a surface that reflects light or other waves back to their source, regardless of the incident angle [33].

The principle involves attaching a tag to the target insect, enabling the reflected waves to be directed back toward the light source. The drone, equipped with both a camera and a light source, illuminates the tag, as shown in the schematic in Fig. 2.10. Due to the tag's reflective property, the camera captures a bright spot on the image, allowing a decision algorithm to update the drone's trajectory and follow the hornet. [33]

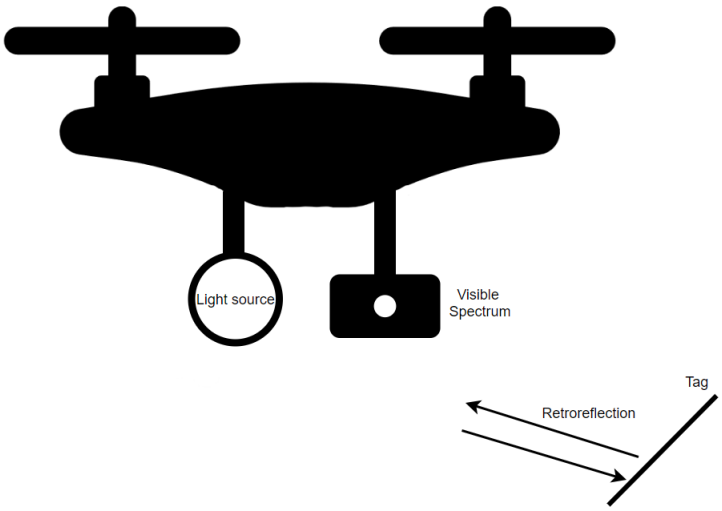

Figure 2.10: Schematic of the principle

The method involves the following steps:

1. Capture the hornet using bait and induce dormancy by cooling.
2. Attach a retro-reflective tag (an example is shown in Fig. 2.11).
3. Release the hornet and initiate drone tracking.
4. The drone automatically follows the hornet using the bright spot detected by the camera.

Figure 2.11: Example of tag retroreflective on bee from [33]

During the experimental period, detection rates varied with distance, with 17 out of 24 tags detected at 30 meters and 18 at 39 meters. As illustrated in Fig. 2.12, the effectiveness of this method is highly sensitive to several factors, such as obstacle reflections that can interfere with visibility and weather conditions that significantly impact performance. While this technique can be very effective in agricultural settings with minimal obstacles and reflective surfaces, its efficacy diminishes in urban or forested environments where light reflection and physical barriers are more prevalent [33].

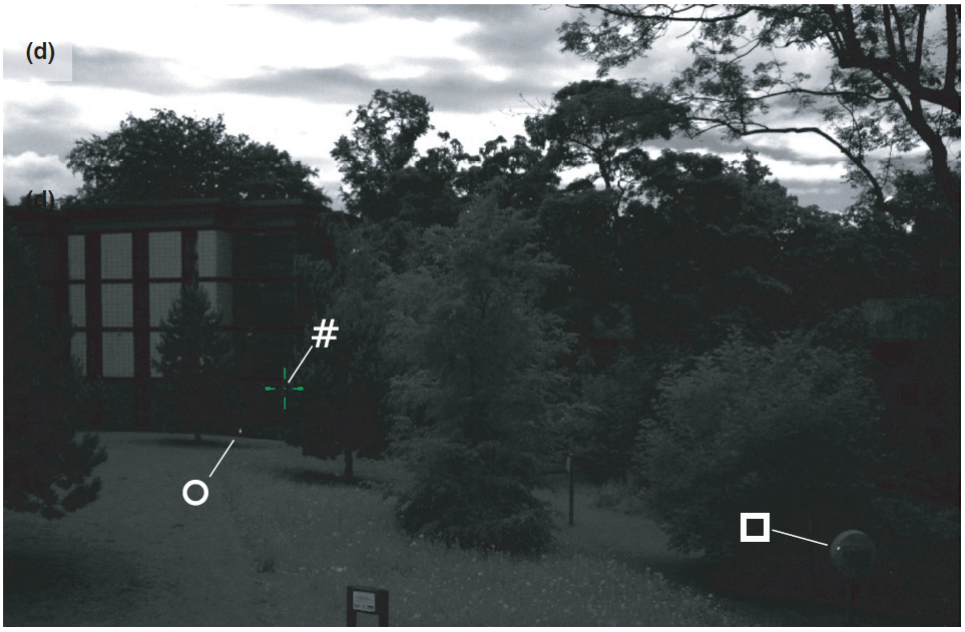

Figure 2.12: Image from tracking system, with the bee detected (#) and examples of other reflections: a lifebuoy cover (□) and the retroreflective material on a traffic cone (o) from [33]

	1	2	3	4	5	6
criteria	★★☆	★★☆	★☆☆	$\leq$ 30m	×	$\approx$ 5mg

Table 2.5: Criteria-based evaluation of retroreflective technology

Radio-telemetry

Instead of utilizing a passive tag, an alternative approach involves employing an active tag that can emit its own signal, simplifying the tracking process. This concept leads to the technology of radio telemetry, which is readily available in the market.

In this approach, the hornet is fitted with an active tag powered by a small energy source, allowing it to emit a detectable signal. The signal is then tracked by an antenna-equipped device that identifies the signal's strength and direction (RSSI), guiding the tracker towards the hornet's location [14]. Fig. 2.13 illustrates examples of this technology.

The methodology consists of the following steps:

1. Trap the hornet using bait and induce dormancy through cooling.
2. Attach the active tag to the hornet.
3. Activate the tag and release the hornet.
4. Track the hornet's movement using the antenna and follow the signal direction.

The radio telemetry system demonstrates significant potential in tracking hornets, with an antenna able to detect the emitted signal from up to 100 meters away

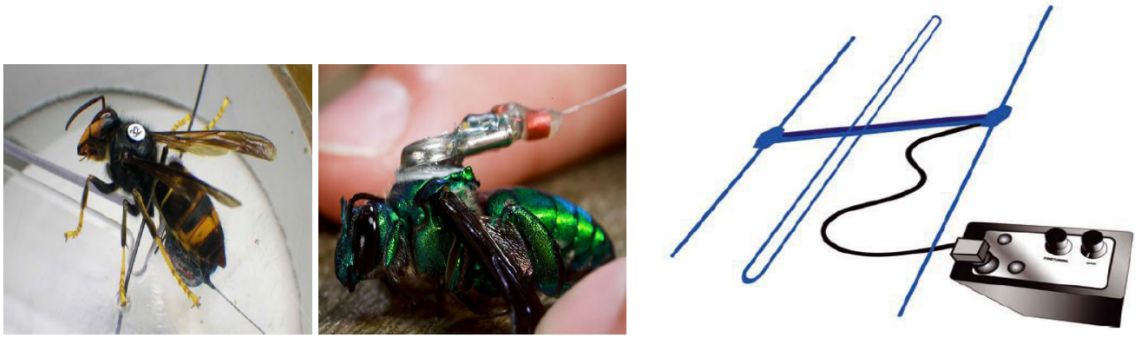

(a) (b)

Figure 2.13: Examples of radio telemetry tracking. (a) Asian hornet and bee with transmitters (b) receiver and Yagi antenna from [16]

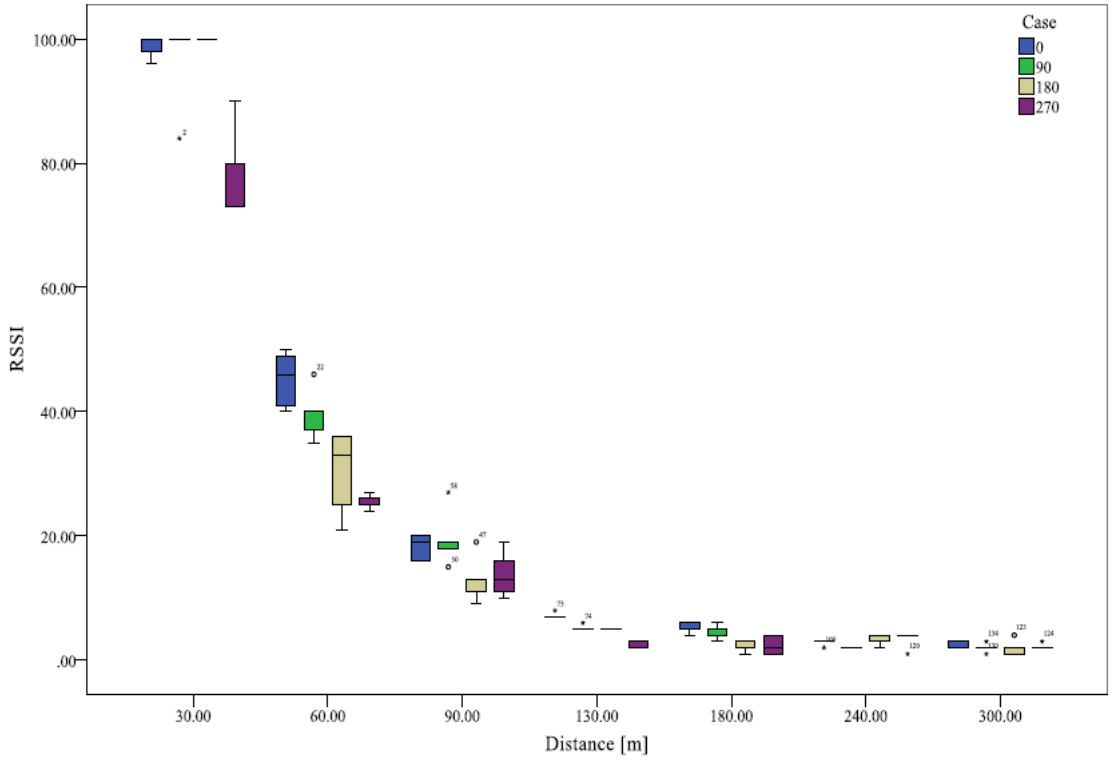

Figure 2.14: Experimental results of the RSSI feasibility test for each distance and angle. [16]

which is shown by the Fig. 2.14. This is promising for effective hornet tracking. However, a practical issue has been observed in a detailed YouTube demonstration [21], where the tag detached from the hornet mid-flight, rendering the tracking effort futile. The search time to locate the tag post-detachment is also extensive, often taking several hours.

The technology must balance constraints such as the tag's weight, surface area, and battery life to ensure it doesn't interfere with the hornet's natural behavior. Given these requirements, a typical tag for this application costs between 170e and 300e and has a battery life ranging from 4 to 7 days, depending on the operational

mode selected [14].

Despite these challenges, the key advantage of radio telemetry lies in its ability to directly pinpoint the hornet's nest in fewer attempts compared to other methods, potentially reducing the overall search time [14].

	1	2	3	4	5	6
criteria	★☆☆	★★☆	★★☆	$\leq$ 800m	✓	$\approx$ 220mg

Table 2.6: Criteria-based evaluation of telemetry

Harmonics Radar

Environmental factors play a crucial role in generating false positives due to the multipath phenomenon, leading to significant degradation in performance. Minimizing this effect is essential. The next proposed technology is harmonic radar, which shares similarities with the previous method but with key differences. The setup remains consistent, involving a radar and a tag, which this time is passive. The distinctive feature of harmonic radar is its ability to receive a signal at the fundamental frequency and retransmit it at the harmonic frequency [2]. The principle is shown in Fig. 2.15.

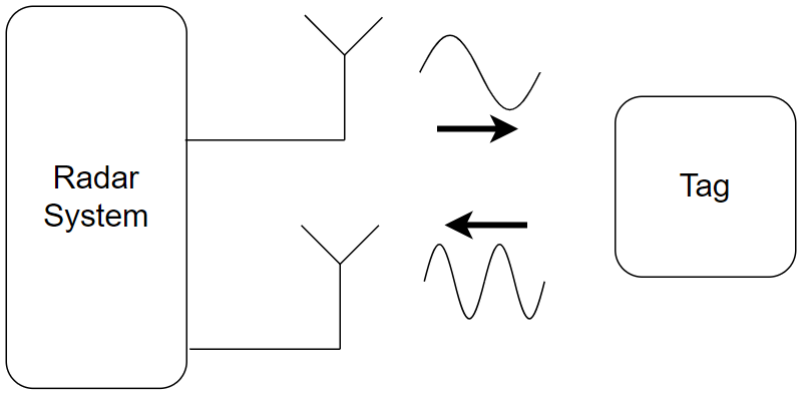

Figure 2.15: Harmonic Radar system overview

This process can be achieved using a nonlinear component such as a diode. This raises the question: what is the relationship between a nonlinear component and the harmonic of a signal? To clarify, we refer to the underlying theory from the book [28].

When a signal is applied to a nonlinear system, the output exhibits frequency components that are integer multiples, known as "harmonics", of the input frequency [28]. Consider an input signal in the form of a cosine wave, x(t) = Acos(ωt) with $0 < A < 1$. The output can be approximated as:

$$
\begin{aligned}
y(t) &\approx \alpha_1 x(t) + \alpha_2 x^2(t) + \alpha_3 x^3(t) \\
y(t) &= \alpha_1 A\cos(\omega t) + \alpha_2 A^2\cos^2(\omega t) + \alpha_3 A^3\cos^3(\omega t) \\
&= \alpha_1 A\cos(\omega t) + \frac{\alpha_2 A^2}{2}(1+\cos(2\omega t)) + \frac{\alpha_3 A^3}{4}(3\cos(\omega t)+\cos(3\omega t)) \\
&= \frac{\alpha_2 A^2}{2} + \left(\alpha_1 A + \frac{\alpha_3 A^3}{4}\right)\cos(\omega t) + \frac{\alpha_2 A^2}{2}\cos(2\omega t) + \frac{\alpha_3 A^3}{4}\cos(3\omega t)
\end{aligned}
\tag{2.1}
$$

From this equation, it is evident that the conversion between the input signal and the output signal's amplitude at the harmonic frequency diminishes rapidly due to the squared term and the $\frac{1}{2}$ factor. Consequently, the radar must emit sufficient power to ensure the re-emitted signal is strong enough to be detected. This requirement necessitates a large transmitting antenna capable of delivering the necessary power. For instance, a study reported a detection range of approximately 125 meters with an output power of 25 kW [24]. The high power output also means that the transmitter system is not negligible, presenting challenges for field deployment, especially if the hornet moves out of the detection range, requiring the process to be repeated. [24]

The advantage of retransmitting the signal at the harmonic frequency is that it allows the receiver to distinguish between true signals and anomalies, primarily caused by the multipath phenomenon due to environmental topology. Fig 2.16 is provided to illustrate this capability.

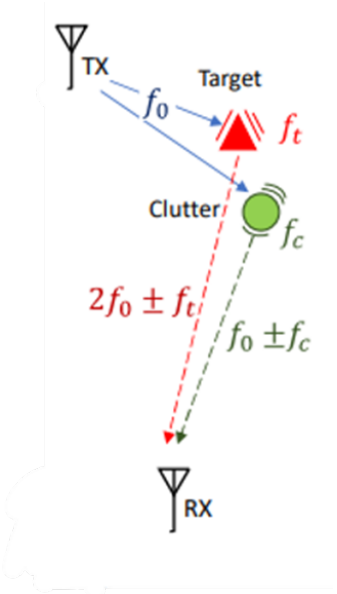

Figure 2.16: Image from [22] representing the reason why this technology resists to environement effects

	1	2	3	4	5	6
criteria	★★☆	★★☆	★★★	$\leq$ 125m	×	$\approx$ 3mg

Table 2.7: Criteria-based evaluation of Harmonic radar

Design choice

Given the requirements outlined at the beginning of this chapter, our goal is to identify a technology that is cost-effective, affordable, and provides acceptable efficiency. Below is a summary of the technologies discussed so far:

Technology	1	2	3	4	5	6
Infrared Imaging	★☆☆	★★★	★★☆	N/A	×	N/A
RFID	★★★	★★★	N/A	$\leq$ 0.5m	✓	N/A
Triangulation	★★★	★★☆	★☆☆	$\leq$ 500m	×	N/A
Retroreflective Tag	★★☆	★★☆	★☆☆	$\leq$ 30m	×	$\approx$ 5mg
Telemetry	★☆☆	★★☆	★★☆	$\leq$ 800m	✓	$\approx$ 220mg
Harmonic Radar	★★☆	★★☆	★★★	$\leq$ 125m	×	$\approx$ 3mg

Table 2.8: Comparison and overview over the different technologies based on defined criteria

The main reason for not pursuing infrared imaging technology is the high equipment cost associated with the extensive deployment of drones required for detecting hornet nests, which contradicts our initial objective of affordability. Similarly, RFID technology is dismissed because, even with an increased detection range, the operational area remains too limited to meet our goals effectively. Triangulation, while effective in locating nests, is excluded due to the high and inconsistent time required to obtain results, making it impractical for our needs. The technology utilizing retroreflective tags is innovative, but its performance is highly dependent on environmental conditions, particularly in areas with significant reflections or adverse weather, making it unreliable in many scenarios.

This leaves us with two viable options: telemetry and harmonic radar. Both technologies are well-suited to the situation, each with distinct advantages. Harmonic radar offers a lighter tag weight and better resistance to environmental factors but suffers from a shorter detection range. Telemetry, on the other hand, provides an excellent range but comes with a high cost. The final decision criterion is the potential of each technology. Telemetry is already commercially available, with established performance metrics, whereas harmonic radar, although still under research, appears more promising for our specific application. Thus, we have chosen to explore harmonic radar, as it shows the most potential for success. To address the challenge of single-process limitations, we propose to use a drone to enhance the effectiveness of this technology.

Chapter 3

System analysis

In this chapter, we begin with a review of the fundamental concepts of radar systems. Following this, we delve into the technology of harmonic radar, providing a detailed explanation of its operating principles. We then specify and justify the parameters chosen for our system, highlighting the criteria and technical considerations that informed our decisions. Finally, based on these parameters, we compute the predicted detection range using a link budget analysis.

3.1 Radar Basics

RADAR stands for "Radio Detection And Ranging". Radars are electromagnetic sensors used for contactless detection, locating, and positioning of one or more objects, commonly referred to as targets. These targets can be anything that reflects electromagnetic waves, such as aircrafts, ships, vehicles, or even animals and insects.

3.1.1 Operating principle

A basic primary radar system can be described as a system composed of a transmitter and a receiver.

The radar transmitter emits signals required for target detection in the form of radar waves, which travel at the speed of light and are imperceptible to humans. Radar transmitters can be built using different waveforms, such as continuous wave (CW) or pulsed, depending on the application. CW radar transmitters, as the name suggests, continuously transmit an RF signal, meaning the system is always active. In contrast, pulsed radar transmitters are designed to produce ultra-high peak RF powers for a short period, making the system active only during this interval and inactive for the remaining time. Some modulation techniques can be applied to CW and pulsed transmitters by modulating the amplitude, phase, or frequency [2]. Further information about CW and pulsed radars will be discussed later in this chapter.

Regarding the location aspect, two scenarios are possible as shown in Fig. 3.1. The first scenario involves the target being directly coupled to the transmission system, where it acts as the source of the transmitted signal. In this case, the only

requirement is for the receiver system to detect this signal to locate the target.

The second scenario is more complex. It relies on the target having an element that can reflect the signal it receives. In this case, the signal is initially transmitted by our system, and upon striking the target, it is altered and reflected back to the sensor, much like an echo. A radar receiver is then responsible for capturing these reflected waves.

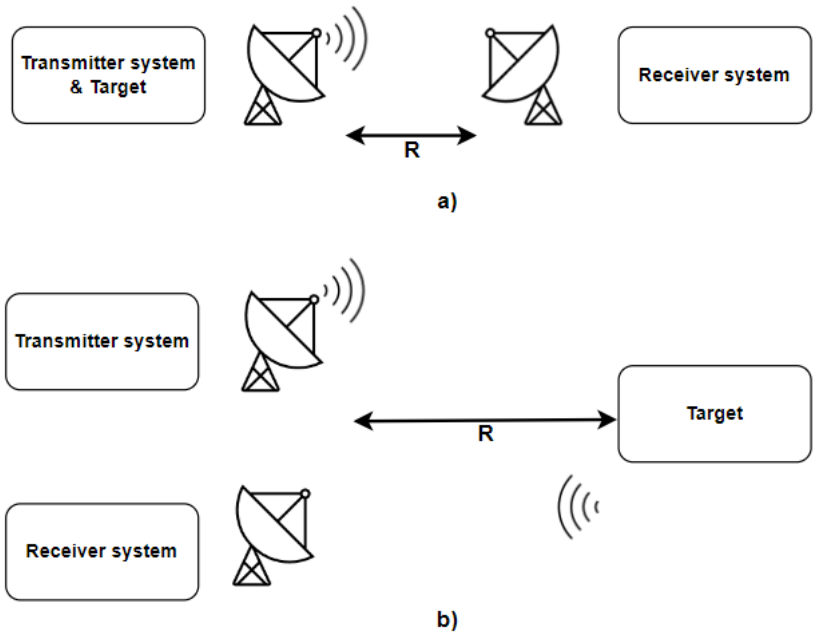

Figure 3.1: Different scenarios (a) signal travel one way and (b) signal back and forth

The advantage of the scenario Fig. 3.1a is that the signal is only exposed once to the undesirable effects of the environment, allowing more reliability on it, whereas in scenario Fig. 3.1b it is exposed twice, reducing its intensity and introducing several random factors on the signal received at the end. The main disadvantage is that the transmission system is coupled to the target. It has to be able to generate a powerful signal in order to be detected, so there is no escaping the need for a battery. This, in turn, imposes a weight and surface constraint on the target. In scenario Fig. 3.1b, on the other hand, there is no obligation to use a battery, which gives us a wider target audience.

3.1.2 Concept

The ability of the radar to perform detect a target relies on the reflected power from targets, they must be large enough to be identified by the radar receiver. To understand and quantify this, we need to introduce several key concepts.

Isotropic antenna

An isotropic antenna is a theoretical antenna that radiates equally in all directions with the same intensity. The antenna has a gain of 1 (0dBi) in the spherical space all around it. An isotropic antenna is usually used as a reference antenna to evaluate antenna gain.

Antenna Gain

Every antenna has a gain, defined as the ratio of the radiation intensity in a given direction to the radiation intensity that would be produced if the same power were radiated isotropically. The concept of gain applies differently to various parts of the system. For a transmitting antenna, gain indicates the efficiency with which the antenna converts input power into radio waves directed towards a specified area. For a receiving antenna, gain describes the efficiency with which the antenna converts incoming radio waves from a specified direction into electrical power. The antenna gain can be calculated using the antenna's effective area A_e, which is the functional (not real) area that an antenna presents to an electromagnetic wave it receives.

$$G = \frac{4\pi A_e}{\lambda^2} \tag{3.1}$$

EIRP

The term "Effective Isotropic Radiated Power" (EIRP) refers to the power level that a signal would reach if it were transmitted by an isotropic antenna. The EIRP is defined as the transmitted power multiplied by the antenna gain.

For calculating the incident power on the reciving antenna, we must first calculate the transmitted power density,denoted as Q_i. For an isotropic transmitting antenna, the power density is uniformly distributed over the surface area of the surrounding sphere. This distribution is inversely proportional to the square of the distance from the antenna. The formula is as follows:

$$Q_i = \frac{EIRP}{4\pi R^2} = \frac{P_t G_t}{4\pi R^2} \tag{3.2}$$

- P_t is the output power given to the antenna
- G_t is the transmit antenna gain
- R is the distance to the receiving antenna

Now that we have established the power density at a distance R from the transmitting source, the power received by a receiving antenna is determined by multiplying this available power density by the effective area of the antenna. Consequently, the radar received power can be expressed as:

$$P_r = \frac{P_t G_t A_e}{4\pi R^2} = \frac{P_t G_t G_r \lambda^2}{(4\pi R)^2} \tag{3.3}$$

The previous equation defines the received power at a distance R from the transmitter, as illustrated in Fig. 3.1a. The assumption that power decreases inversely proportional (following an inverse square law) to the distance holds true only when the receiving antenna is situated in the far field of the transmitting antenna and also there are no multipath effect. To determine the distance at which the far field begins, the following formula is applied [43]:

$$\text{Far Field} \geq \frac{2D^2}{\lambda} \tag{3.4}$$

Where D corresponds to the diameter in the case of circular antenna and the height if not.

However, we are particularly interested in the scenario where the signal propagates to a target and is reflected back with a reflection coefficient, σ ranging between 0 and 1. The signal then travels the same distance back to the radar receiver, as depicted in Fig. 3.1b. In this situation, the radar received power can be perceived as :

$$P_r = \frac{P_t G_t \lambda^2}{(4\pi R)^2} \frac{\sigma G_r \lambda^2}{(4\pi R)^2} \tag{3.5}$$

Again, the formula is valid only if the target is in the far field of the antennas.

Detection range

Radars operate by transmitting a known electromagnetic wave and then detecting its reflection from nearby objects, as described in earlier section. Since electromagnetic waves travel at the speed of light, the distance to the target can be determined by measuring the time it takes for the wave to return to the radar receiver. The following equation is used to calculate this distance based on the round-trip time of the EM wave.

$$R = \frac{c\Delta t}{2} \tag{3.6}$$

Where

- c is the speed of the light
- Δt is the time needed to complete this distance

However, another critical factor to consider is noise. Due to the various components that make up antennas, the radar receiver generates white gaussian noise with uniform power spectral density. Target detection is limited by this receiver noise. To effectively detect a target, the reflected signal must be significantly stronger than the noise power, as determined by the required Signal-to-Noise Ratio (SNR) of the receiver [2]. Noise is composed of 2 parts. The first is the minimum equivalent input noise for the receiver at temperature T_s and can be calculated from the following formula:

$$P_{noise,input} = kBT_s \tag{3.7}$$

Where

- k is the constant of boltszman
- B is the bandwidth of our signal

The second part is the noise figure which can be interpreted as the noise generated by the antenna components, which adds to the input noise. This value is generally expressed with logarithmic scale.

$$P_{NoiseFloor} = P_{noise,input,dBm} + \text{NoiseFigure} \tag{3.8}$$

To be detectable by the radar signal processor, the SNR must be greater than 1, typically with an additional margin specified by system requirements. The SNR can

be calculated by dividing the radar's received signal power by the receiver's noise power, as follows :

$$SNR = \frac{P_r}{P_{NoiseFloor}} \tag{3.9}$$

3.2 Harmonic Radar

The name derives from the fact that the radar's received frequency is at the second or third harmonic of the transmitted signal frequency. To achieve this, a small nonlinear element, such as a diode, is used to generate the harmonic frequency of the signal. Additionally, an antenna that resonates at both the transmit and receive frequencies is required at the target, allowing the appropriate signal reflections to be directed back to the radar receiver. The combination of the diode and antenna, placed on the target of interest, is known as the tag.

The tag is powered by the radar's transmitted electromagnetic wave, eliminating the need for a battery or any other energy source. This feature significantly reduces the tag's size and weight requirements so it can be attached to a ski boot, helmet, or even a tiny insect or human using adhesive tape.

Additionally, the technology offers immunity to environmental effect such as multipath because the signal generated by the target occurs at a harmonic frequency. In contrast, reflections from the surrounding environment typically occur at the fundamental transmission frequency, allowing the radar system to distinguish the target signal from background noise more effectively as shown in Fig. 2.16.

This techonology is mainly used in the situation shown in Fig. 3.1b. Therefore the expression for the power received at the harmonic frequency by our receiving antenna (3.5) becomes :

$$\begin{aligned} \frac{P_{RX,h}}{P_{TX,f}} &= \frac{\eta G_{TX,f} G_{RX,f} \lambda^2}{(4\pi R)^2} \frac{G_{TX,h} G_{RX,h} (0.5\lambda)^2}{(4\pi R)^2} \\ &= \frac{1}{4}\eta \underbrace{G_{TX,f} G_{RX,h} G_{RX,f} G_{TX,h}}_{G_{total}} \frac{\lambda^4}{(4\pi R)^4} \end{aligned} \tag{3.10}$$

Where

- $P_{TX,f}$ is the radar transmitted power at the fundamental frequency
- $P_{RX,h}$ is the radar received power at the harmonic frequency
- $G_{RX,f}$ is the tag antenna gain at the fundamental frequency
- $G_{TX,f}$ is the radar transmit antenna gain
- $G_{RX,h}$ is the radar receive antenna gain
- $G_{TX,h}$ is the tag antenna gain at the harmonic frequency
- η is the conversion coefficient of the tag

The idea of using this techonology in the context of Asian hornets is to design a compact, lightweight, and low-power harmonic radar system, including both the transmitter and receiver, to be carried by a drone. In order to do that, several constraints need to be fullfilled. Firstly, the tag designed to be fitted on the hornet should not exceed a weight of 0.25g because it has been proven from [14] that using a higher weight that it can alter the natural move of the hornet and hence the probability that it go back to the nest is drastally reduced. This is the same case for the dimension of the tag. The contact surface must be compatible with the size of the hornet, within 3x3cm in order to be able to fix in the back or the thorax. Additionally, minimizing the weight of the radar module is essential so that the drone can adequately support it. For example, in the paper [2], with the drone DJI S1000, the maximum allowed weight is 2kg. Finally, the radar transmissions must adhere to the relevant frequency and radiated power regulations.

State of the art

The technology is still under active research, with a considerable amount of literature already available. Researchers have published numerous papers exploring its potential and various applications, particularly in tracking insects. We present some of these findings below.

Radar system

The functionality of this part of the system has already been described at the beginning of this chapter. The research carried out within this framework has focused on 3 directions. The first is more general: the aim is to achieve maximum range, as this is a direct factor in system performance. Secondly, particular attention has been paid to power consumption and weight, as the aim is to be able to implement this technology on a drone, which is subject to a number of constraints.

The first paper proposes a design for this part of the system, primarily aiming to achieve maximum range at the expense of the other criteria. The design specifies a transmitted power of 74dBm and achieves a detection range of 125m using a radar module weighing 25kg [24].

A second study, concentrating on the last two criteria, developed two prototypes operating at respectively 2.9,5.8GHz and 9.3,18.6GHz. The first prototype detects hornets at a distance of up to 40m with an output power of 33.7dBm, while the second detects up to 15m with a power consumption of 40dBm. Both prototypes are equipped with radar modules weighing 3kg each [35].

Unfortunately, the cited papers provide little information on how the detection range of the system is evaluated. Instead, we are presented directly with experimental values. However, it is crucial to estimate the potential detection range during the design phase of a system. This work introduces a method for approaching this concept using a link budget analysis.

Tag design

As far as the tag is concerned, several factors come into play regarding performance. On the one hand, there is the antenna gain, and on the other, the conversion efficiency of the fundamental frequency signal power to its harmonic frequency. The design of the tag significantly influences these factors. Several research projects have explored this area, with the implementation of a tag featuring a dipole antenna structure being particularly popular.

A first paper presents the design of a tag based on the conventional dipole antenna structure and its performance, as illustrated in Fig. 3.2a. The tag weighs less than 3mg by using by using 150µm diameter copper wire and has a conversion efficiency of 0.8% at 9.4-18.8GHz [6]. Another study at the same frequency, which used the same design but with another diode and 250µm diameter copper wire, reported a conversion efficiency of 0.65% with a weight of 12mg [24].

The paper [18] proposes a different configuration, as shown in Fig. 3.2b. The tag designed in this configuration weighs 60mg. Unfortunately, no information about the conversion efficiency has been reported. However, the performance of this design have been validated by comparing different simulations of the S-parameters on 3 separate Software (ADS, CST, Ansys HFSS).

In the cited papers, there is unfortunately little discussion of the methodology used to bridge the gap between the design of a real circuit and its representation in simulations. Specifically, they do not detail how to transition from one representation to the other. It is crucial that simulations accurately predict the performance observed in reality. This work focuses on taking a tag design concept, implementing it in ADS, and comparing the simulated results with actual performance measurements.

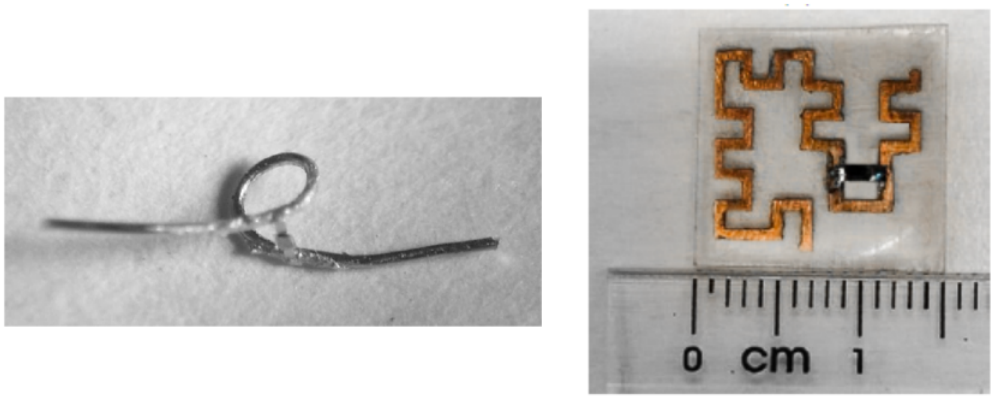

Figure 3.2: Examples of harmonic radar tag. (a) Traditionnal design of dipole antenna from [6] (b) Custom design of dipole antenna from [18]

3.3 Proposed System Specifications

Table 3.1 shows the system specifications considered in the design of the harmonic radar system. The rest of this chapter is dedicated to explain the choice of the parameter.

	Specification	Unit
Frequency	2.9,5.8	[GHz]
Modulation	FMCW	[/]
Bandwidth	500	[MHz]
EIRP	40	[dBm]
Receiver Antenna Gain	26	[dBi]
Transmitter Antenna Gain	20	[dBi]
Noise	-96	[dBm]
SNR	6	[dB]
Conversion efficiency	-55$\leq x \leq$-15	[dBm]
Processing gain	30	dBi

Table 3.1: System Specifications.

3.3.1 Frequency

Now we need to decide on the operating frequency for our prototype. Several factors need to be considered such as IBPT regulation (Institut belge des services postaux et des télécommunications) which regulates radio frequencies in Belgium [11]. Another element to take into account is the atmospheric attenuation which for different frequency bands experience distinct levels of free-space attenuation, as shown in Fig. 3.3. Finally, the last detail to consider is the properties of propagation mechanism such as reflection and scattering which are highly frequency-dependent.

We limit the frequency search area to 1GHz-18GHz. As a general rule, antenna size is inversely proportional to frequency [3], frequencies below 1GHz would be unsuitable for the tag. As for frequencies above 18GHz, this would require more complex systems in terms of resources for the radar part of the system. Hence, It is not be taken into considerations. By investigating the frequency plan provided by ibtp, the various possible uses of frequency for radiolocation are shown in Fig. 3.4.

The choice of frequency is based on several aspect. The trend shown in Fig. 3.3 is that the higher the frequency, the greater the atmospheric attenuation. This is also true of the propagation mechanism: the higher the frequency, the greater the distance losses.

That is why we are interested in low frequencies. A first choice would have been to use the 1.2GHz-2.4GHz frequencies, but the 2.3GHz-2.5GHz frequency band has various applications that can induce interference. We therefore decided to discard it.

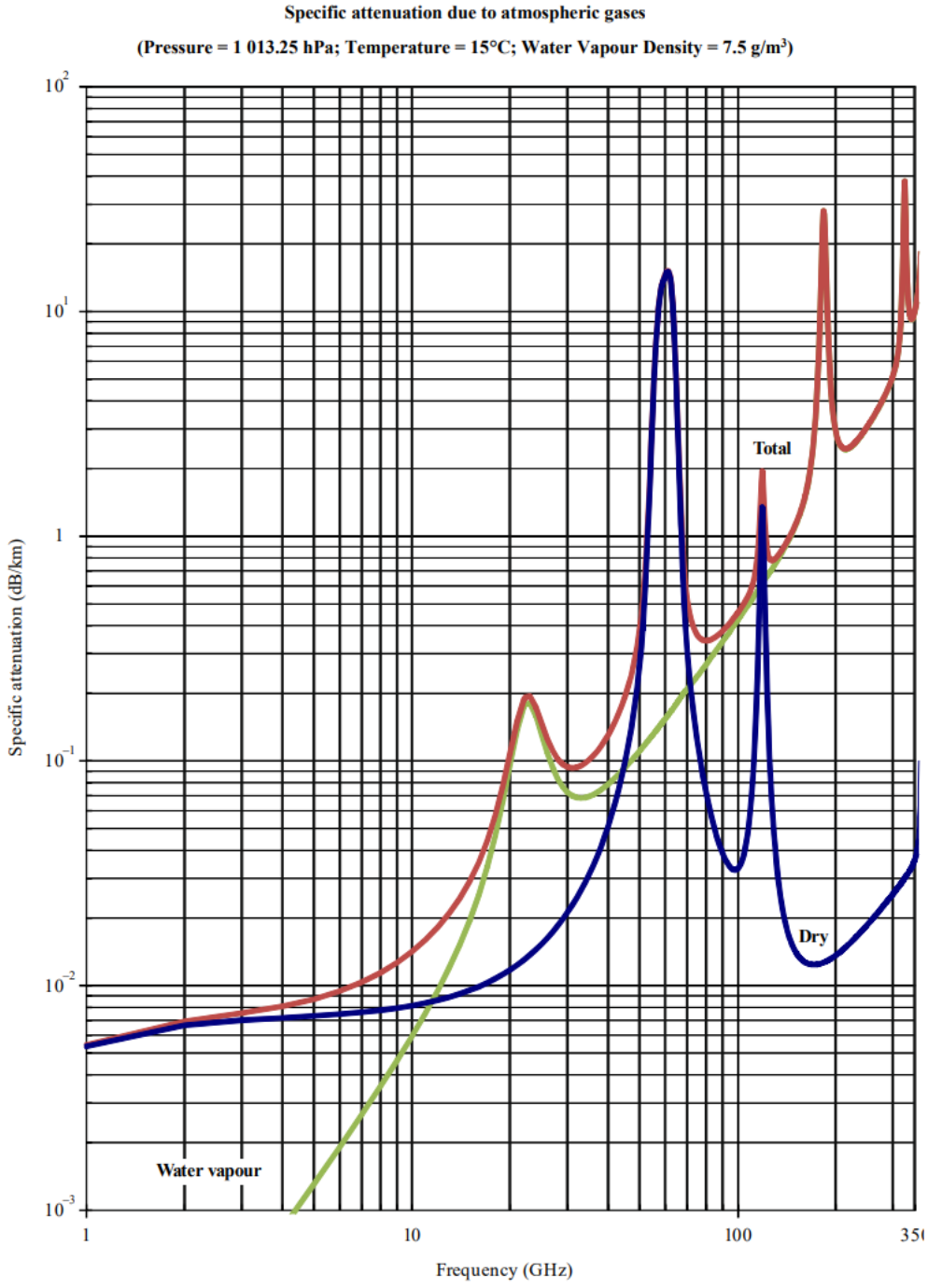

Figure 3.3: Atmospheric Attenuation Over Frequency Bands from [13]

The next choice would be to choose frequencies in the band 2.7GHz-2.9GHz for the fundamental and 5.4GHz-5.8GHz for the harmonic. In the design proposed in the paper [35], they use the frequency range of 2.9,5.8 GHz. It would be interesting to choose the same frequencies so we can compare the performance of the system across the remaining sections. Hence the operating frequencies are 2.9GHz and 5.8GHz.

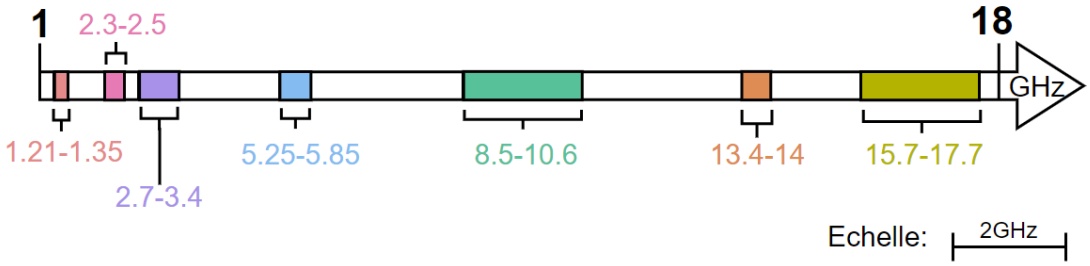

Figure 3.4: IBPT

3.3.2 Modulation

In this application, our objective is to recover weak signals by utilizing the correlation between the known outgoing signal and the received signal from target reflections. To achieve improved results, such as increased detection range, it is essential to design a modulation that satisfies all system requirements. The two primary types of radar waveforms are pulsed-wave radars and continuous-wave (CW) radars [2].

Pulsed Radar

Typically, a pulsed radar uses a single antenna for both transmission and reception. During the transmission phase, the radar emits signals only within the pulse duration,x, meaning the receiver is turned off. Immediately after, during the echo or listening duration, the radar receiver becomes active. The Pulse Repetition Interval (PRI) is the combined length of these two durations and defines the sequence of transmission (TX) and reception (RX) times, which repeats consistently during operation as shown in Fig. 3.5 [2].

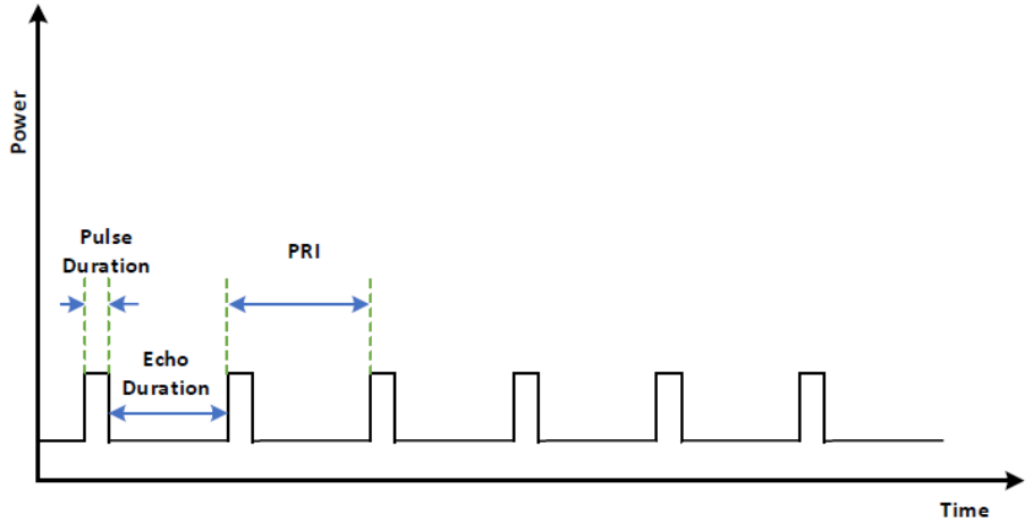

Figure 3.5: Pulse radar waveform from [2]

Range measurement with pulsed radars is achieved by calculating the round-trip time ΔT of the reflected radar signal from the target, as shown in (3.6). Since the

receiver is only active during the listening duration, it cannot detect reflections from targets that are very close, with ΔT falling within the transmission period (x). This limitation establishes the minimum detection range of the pulsed radar.

$$R_{min} = \frac{c \cdot x}{2} \tag{3.11}$$

The undetectable range below R_{min} is known as blind range of the radar. It depends on the radar pulse duration, meaning that choosing this factor involves a trade-off between achieving higher average power and minimizing the detection range [2].

Radar maximum range R_{max} is a function of the PRI. It can be found as

$$R_{max} = \frac{c \cdot PRI}{2} \tag{3.12}$$

The maximum unambiguous range of the radar is defined as the range that can be resolved within a single PRI. Targets detected beyond this range R_{max} is registered in the subsequent PRI, resulting in an ambiguous range. Therefore, the PRI must be designed to be sufficiently long to accommodate the farthest targets of interest, thereby avoiding range ambiguity [2].

$$PRI_{min} \geq \frac{2R_{max}}{c} \tag{3.13}$$

FMCW

A continuous wave (CW) radar transmits and receives data continuously, naturally it uses 2 antennas for this purpose. Range measurements in non-modulated CW radars are ambiguous because the returns cannot be referenced to the transmission times, making it impossible to calculate signal round-trip times. To measure range, a CW radar must modify the transmitted wave to enable identification of signal returns. One widely used technique for this purpose is Frequency Modulated Continuous Wave (FMCW) radar [2].

An FMCW radar generates a frequency-modulated continuous wave signal for transmission. The transmit frequency is continuously swept across a frequency range known as the sweep frequency, f_{sweep}, to achieve modulation. The transmitter must complete a full f_{sweep} within one sweep duration, T_{sweep}. The radar receiver then compares the reflected target signal with the currently transmitted radar signal to produce a difference frequency called the beat frequency, f_{beat}. Some design of frequency variation are shown in Fig. 3.6 [2].

The range depends on the f_{beat} but also the slope of the transmitted chirp S which can be calculated by using the following equation:

$$S = \frac{f_{sweep}}{T_{sweep}} \tag{3.14}$$

Using the measure beat frequency and the transmitted chirp's slope, the round-trip time ΔT of the reflected signal from the target can be computed as follows:

$$\Delta T = \frac{f_{beat}}{S} \tag{3.15}$$

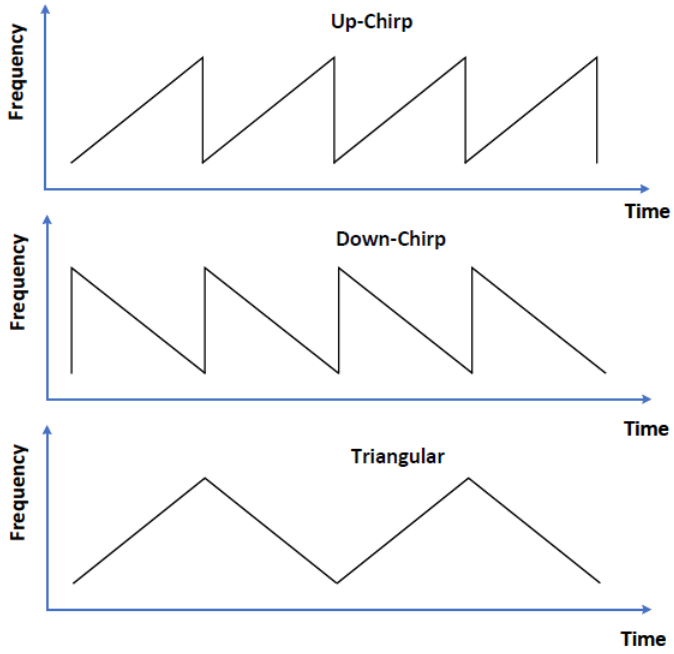

Figure 3.6: Examples of possible frequency variation from [2]

The target range can be calculated using (3.6), along with the slope of the chirp and the beat frequency.

$$R = \frac{\Delta T c}{2} = \frac{f_{beat} \cdot c}{2 \cdot S} \tag{3.16}$$

The minimum range R_{min} of an FMCW radar is ideally zero if the receiver can detect very small frequency drifts. This offers an advantage over pulsed radar, as the minimum range is independent of the system bandwidth. The maximum range R_{max} of an FMCW radar is determined by the chirp signal sweep time T_{sweep}. To identify more distant targets, T_{sweep} should be longer than the round-trip duration of the reflected signal from the furthest target, ΔT [2].

Using a continuous wave design requires two separate antennas: one for transmission and one for reception. However, this design offers a 100% dutycycle and ideally no blind range, which align with our objectives. Comparing the two different designs, FMCW is more suitable for our application.

3.3.3 Bandwidth

In the case of FMCW, a higher bandwidth increases the range of the f_{sweep} and hence the slope S. According to the Equation (3.16), a large bandwidth enhances the accuracy of the estimated distance between the target and the antenna. However, according to Equation (3.7), it also means that a greater power of the noise. Therefore, we need to find a trade-off between these two factors. Considering these aspects, we selected a noise power bandwidth of 500MHz, as it has also been chosen in [2] resulting in a noise power value of -96dBm by using the Equation (3.7).

3.3.4 Belgian standards for EIRP

There are national and european standards that regulate the electromagnetic radiated power. European standards are based on ICNIRP guidelines. According to this, the maximum power density we can achieve for the frequencies of interest is $10\text{W}/m^2$.[7]

Belgium is divided into three regions, each with its own standards to limit exposure to radiation from stationary transmitting antennas . In Wallonia the standards apply to fixed transmitting antennas with an output power greater than 10W. To avoid being restricted by these various regulations, we have decided that our device cannot exceed this power limit [20].

3.3.5 Antenna Gains

In our application, we aim for a high gain value to maximize the detection range. Although higher gain results in a narrower beam, this is acceptable since the antennas are mounted on a drone, which can be maneuvered in both the azimuth and vertical planes.

Regarding the dipole antenna equipped on the tag, we assume a gain of 0dBi, although we know this is not entirely accurate. In reality, the gain is low, approximately in the range of 1-2.55dBi.

3.3.6 SNR

Here, to ensure a good probability of signal detection after processing gains, we set the SNR value at 6dB above the noise level. This value is taken from document [2].

3.3.7 Conversion efficiency

To understand this notion, we investigate the operation of a tag by examining the prototype discussed in paper [35]. The principle is illustrated in Fig. 4.1 and the circuit layout is shown in Fig. 3.7a. The signal at the fundamental frequency is received by the antenna on the left and delivered to the rest of the circuit. The T-circuit functions as an impedance matching circuit, optimizing the power transfer from the receiving antenna to the diode. Due to the diode's nonlinear behavior, it generates the harmonic of the signal, which then propagates through the right side of the circuit. Similarly, a second T-circuit, also serving as an impedance matching circuit, maximizes the power transfer to the transmitting antenna.

The performance is influenced by several factors, including harmonic generation by the nonlinear element, impedance matching and antenna coupling. Collectively, these phenomena are defined as conversion efficiency, CE.

Fig. 3.7b represents a comparison between simulation results and expected results. The latter is mainly based on 2.1. The power of the harmonic output signal is proportional to the square of the power of the input signal. Hence the CE depends

on the incident power level of the tag. We define mathematically the CE by the 3.17.

$$\text{Conversion efficiency} = \frac{P_{TX,h}}{P_{RX,f}} \tag{3.17}$$

Where

- $P_{TX,h}$ is the tag transmitted power at the harmonic frequency
- $P_{RX,f}$ is the tag received power at the fundamental frequency

The data of Fig. 3.7b is used as CE in the remaining section in this chapter. A more detailed analysis will be conducted in the next chapter.

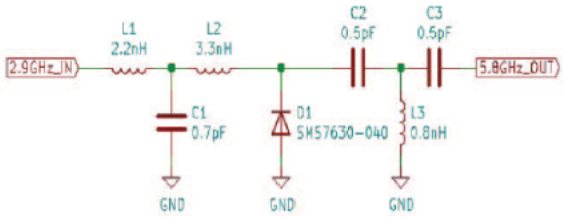

(a) Diode test circuit with diplexer

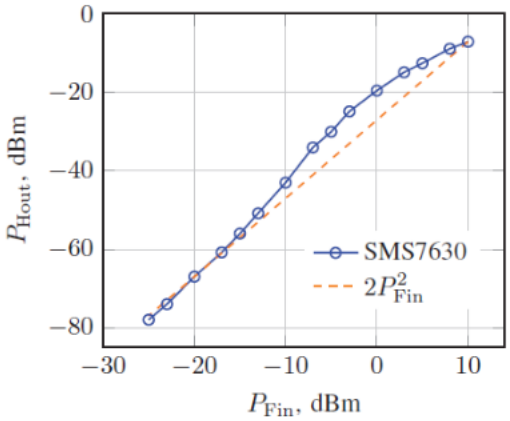

(b) Diode conversion loss

Figure 3.7: Evaluation of the conversion loss of the diode SMS7630-040 at 2.9-5.8GHz (a)Simulation circuit (b)Simulation performance from [35]

3.3.8 Processing Gain

Processing gain refers to the application of specific signal processing techniques to enhance the SNR.

In our case, achieving a high processing gain would allow us to detect targets at greater distances. However, the higher the processing gain, the more number of points to perform the FFT is needed, hence the more complex the system becomes, requiring a trade-off. According to the document [2], a system designed for drone deployment achieves a processing gain of over 30dBi. We have therefore set our processing gain to this value. The analysis of the transmitter and receiver systems is not covered in this work.

3.3.9 Propagation model

To develop an accurate model, it is essential to estimate the signal power losses due to distance. In an unobstructed environment, the free-space path loss model is appropriate for this purpose. This model is based on the Friis formula and is valid

only when the target is in the far field of the antenna, as explained in 3.4. The model is characterized by an exponent of 2 in the following formula:

$$\text{FreeSpacePathLoss} = (\frac{4\pi R}{\lambda})^2 \tag{3.18}$$

In environments with obstacles, the transmitted signal experiences greater attenuation, and the exponent value increases depending on the specific conditions.

3.4 Link Budget

With the system parameters defined earlier, we now focus on determining the maximum detection distance the proposed system can achieve. This involves performing a link budget analysis to ensure that the system, with all its selected components, functions as required. Specifically, this means verifying that the received signal strength is sufficient for the communication system to be detected at the receiving antenna. This is achieved by calculating the power at each stage of the system, as illustrated in Fig. 3.8 and ensuring that the SNR at the final stage of the radar receiver remains above a threshold derived from the system requirements.

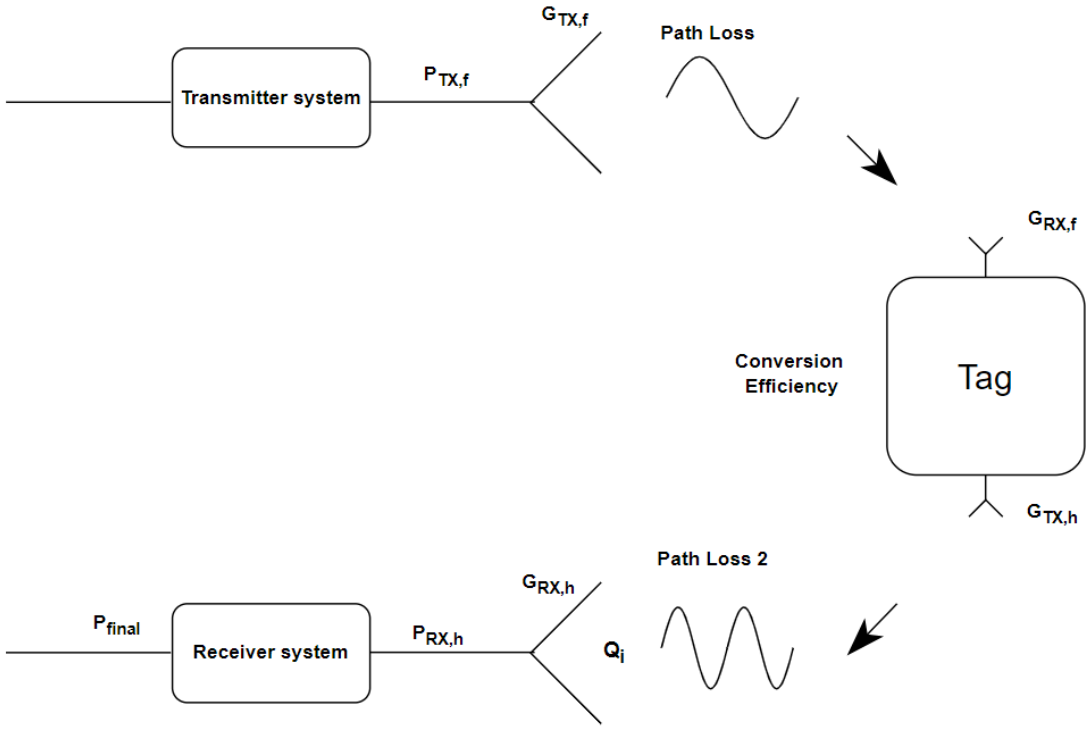

Figure 3.8: Communication scheme

The radar range equation 3.10 becomes:

$$P_{r,dBm} = P_{TX,f,dB} + G_{total,dBi} + 40log_{10}(\frac{\lambda}{4\pi R}) + 30dB \tag{3.19}$$

And the receiver noise power in 3.7 becomes:

$$P_{NoiseFloor,dBm} = 10log_{10}(kBT_s) + 30dB + \text{NoiseFigure} \tag{3.20}$$

The addition of 30dB shifts the reference from dB to dBm. We also made the assumption that the NoiseFigure of the receiver is set to 2dB, value chosen arbitrarily. The receiver SNR in 3.9 becomes:

$$SNR_{dBm} = P_{r,dBm} - P_{NoiseFloor,dBm} \tag{3.21}$$

With these formulas, we can determine the power received by the receiving antenna over a given distance, accounting for parameters such as the propagation model and the variable CE, which changes accordingly. We define the minimum power level required for detection, based on our system requirements:

$$P_{r,dBm,sensitivity} = SNR_{dBm} - G_{Processing} + P_{NoiseFloor,dBm} = -118 \tag{3.22}$$

Fig. 3.9 illustrates the results over distance with the EIRP fixed to 40dBm.

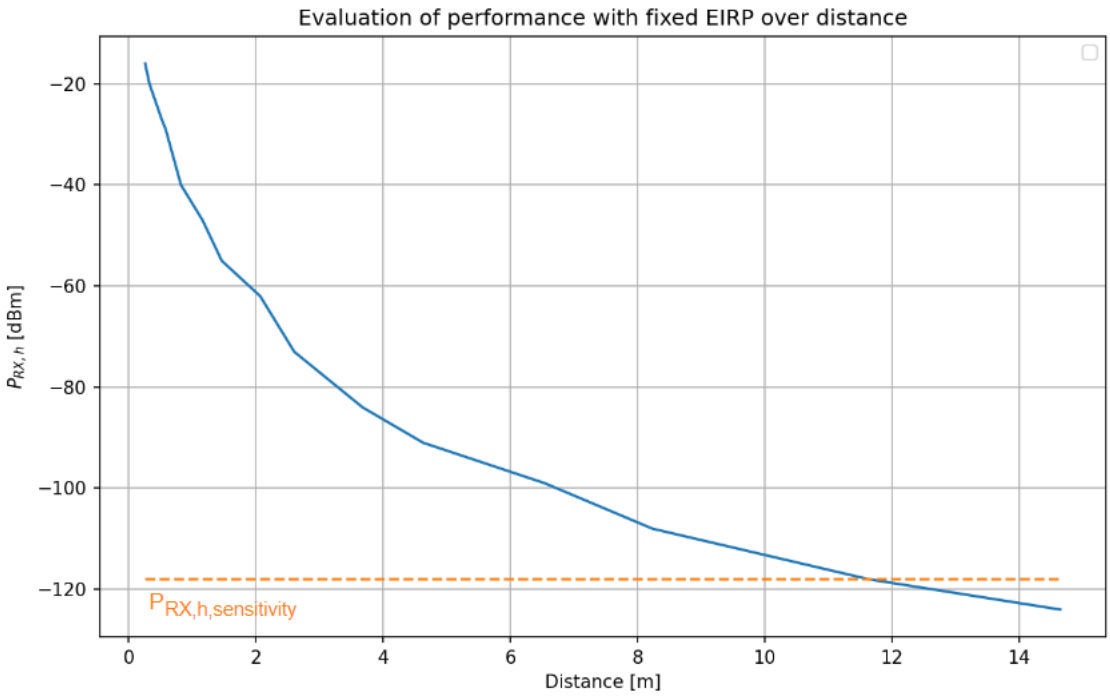

Figure 3.9: Received power at harmonic frequency over the distance

Fig. 3.9 indicates that the maximum detection distance our system can achieve is approximately 12m. To understand the factors contributing to this result, we examine the link budget in more detail using Fig. 3.10.

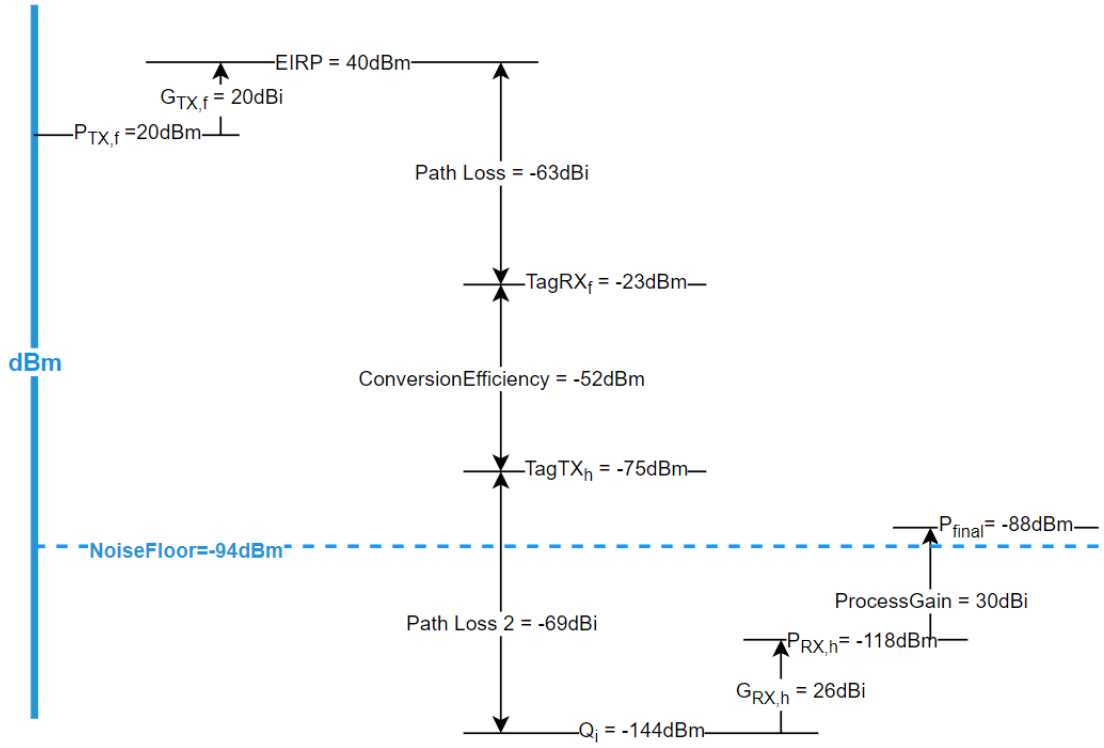

Figure 3.10: Link budget for a distance of 12m

We found that distance to be unsatisfactory. Without altering the transmitting power, we focus on identifying parameters that could enhance performance, specifically by increasing the detection range. We have two main options: improving gains or minimizing losses. We prefer the latter approach. Since path loss is unavoidable, the primary focus is on improving the conversion efficiency, which accounts for one-third of the total losses. Therefore, we investigate the tag further to optimize it.

Chapter 4

Tag design

The tag is used to highlight the target of interest, which in this case is the Asian Hornet, to the harmonic radar amidst the surrounding environment. This is achieved by designing a special antenna in conjunction with a nonlinear RF element to reflect the radar wave at the second harmonic frequency.

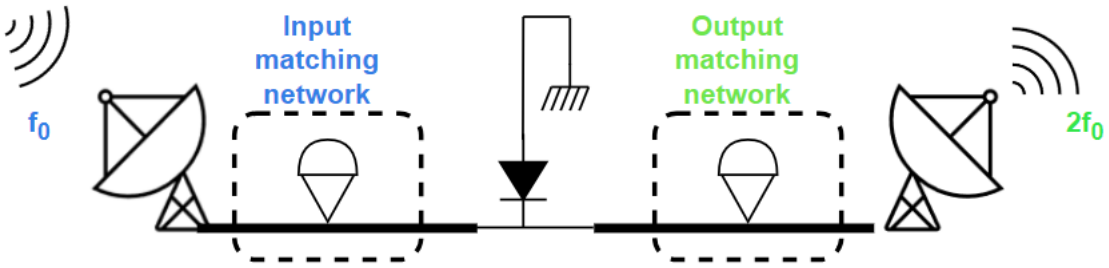

Figure 4.1: Representation of tag functions

In our application, the nonlinear component is a Schottky diode, chosen for its very low forward voltage threshold, which enables the detection of weak RF and microwave signals. As shown in Fig. 4.1, the configuration primarily relies on the diode, but also depends on various factors such as the IN and OUT matching circuits and the choice of antennas. These elements influence the overall loss of harmonic transponders, which in turn determines the transponder's detection range. Therefore, selecting an appropriate diode is the a first critical aspect of designing a transponder.

4.1 State of the art

Over the past few decades, extensive research has been conducted in this field using various type of diode, leading to a better understanding of their performance and potential applications. This research is summarized in Table 4.1.

It has been observed that the SMS7630, popular in low-power energy rectifier designs, has been commonly used for building passive harmonic transponders in recent years. This is one of the reasons why it has been chosen in this chapter. Additionally, we aim to compare the performance of the selected diode with another

Number	Diode	Year/Paper
1	SD101BWS-7-F	2003/[5]
2	SMS7630-040LF	2020/[35] and 2015/[24]
3	SMS7621-040LF	2011/[37]
4	HSCH-5336	2013/[4]
5	HSCH-5340	2008/[27]

Table 4.1: List of diode used in the design of tag in scientific paper over recent years

potential candidate. To do this, the features of the diodes from the literature are compared in Table 4.3.

Parameters	1	**2**	**3**	4	5
Weight[mg]	4	0.6	0.6	N/A	N/A
Frequency[GHz]	N/A	0-24	0-24	1-26	1-26
Size[mm]	1.8x1x1.4	1x0.46x0.6	1x0.46x0.6	0.7x0.27x0.06	0.7x0.27x0.06
Unit price	0.34€	0.56€	0.56€	N/A	N/A
Market	✓	✓	✓	×	×

Table 4.2: Comparison of diode from literature

The first diode, despite its low mass, is not considered because its operating frequency range is unspecified. While it might function across a broad spectrum of frequencies, we prefer diodes that are designed for specific frequencies. This preference is based on the general principle that a system tailored for a particular frequency range is likely to deliver superior performance compared to a more generalized system.

The last two diodes, though operating within the desired frequency band, are discarded because their lifecycle are obsolete and this are no longer in the market.

Given the popularity of the second diode architecture in recent years and its defined frequency of operation, it is expected to provide more reliable and efficient performance. Therefore, we we have chosen the SMS7630 for our design.

Additionally, the SMS7621 has been identified as a potential candidate that may outperform the SMS7630 for transponder design. Comparative studies documented in the literature provide insights into the performance differences between these two diodes, further supporting the selection of the SMS7621. These studies suggest that the SMS7621 may offer advantages in terms of conversion efficiency, power efficiency, and other critical parameters relevant to our application. Therefore, considering these aspects, we have decided to use the SMS7621 in our design. [10]

Since the choice of the tag is not the only factor influencing system performance, we want to examine the tags that have been developed in recent years. Fig. 4.2 presents various designs, and Table 4.3 lists the corresponding characteristics.

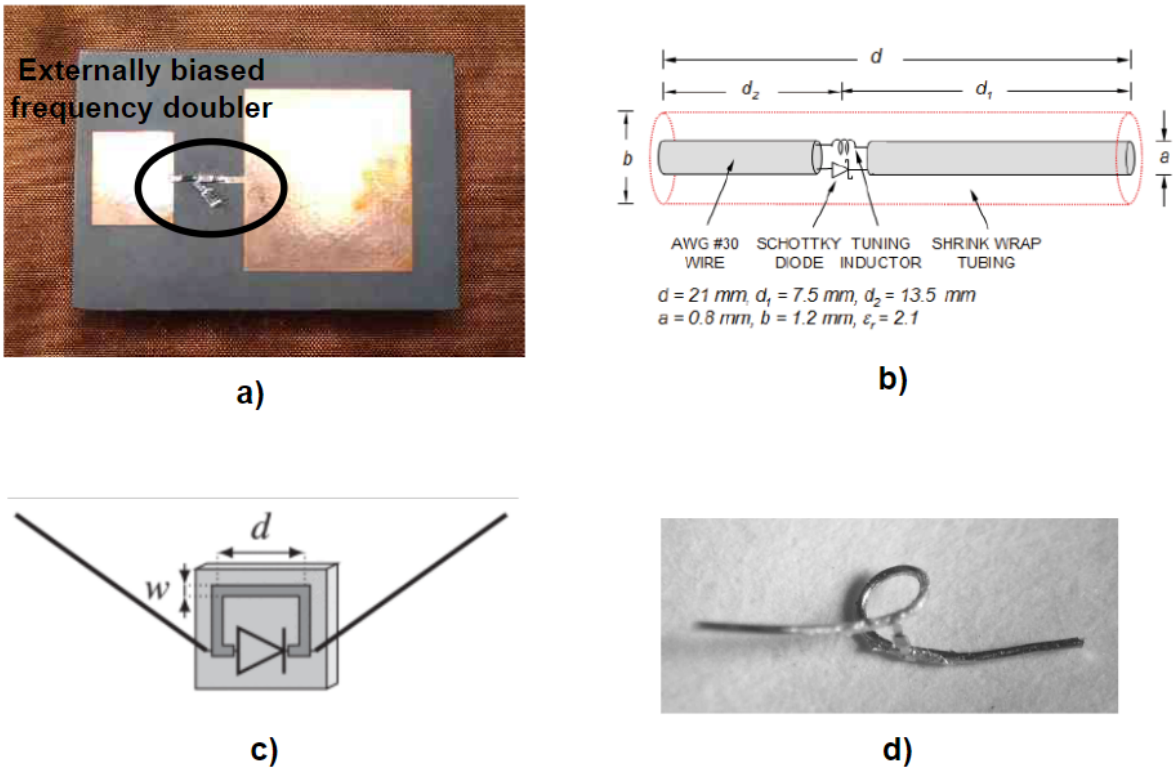

Figure 4.2: Different tag designs : a) Microstrip antennas with externally biased frequency doubler from [4] b) Sleeved harmonic tag with unequal arms from [37] c) Hybrid V-shaped tag with a square-printed loop from [19] d) Dipole antenna with inductive loop from [6]

The first design was developed primarily to minimize the transponder's impact on the insect and to address polarization loss. This issue can be resolved by using microstrip antennas. These antennas, when operating at a sufficiently high frequency, are small enough to be attached to the insect's thorax without hindering its natural movements, obstructing wing function or causing significant aerodynamic drag [4].

The third design offers several advantages. By incorporating a printed base for the diode and tuning inductance circuit, it significantly simplifies the placement of the diode compared to a fully wire-based tag and protects it from potential mechanical disturbances caused by the insect's movements. Additionally, it allows for precise implementation of the tuning inductance, which is fully controllable, reproducible, and can be evaluated numerically before deployment. The printed base also serves as a platform for attaching the tag to the insect [19].

The final design includes an inductive loop to counteract the electrostatic charge distribution that can occur between the two halves of the transponder due to the diode's rectifying action. This charge could be strong enough to bias the diode into a non-conducting state, so the inductive loop was added to mitigate this effect. The second reason is that it can protect the very sensitive diodes from accidental exposure to potentially damaging electrostatic voltages during handling in the field. [30].

Configuration	Size [mm]	Poids [mg]	CE [dBi]	Frequencies [GHz]	Diode
a)	N/A	N/A	-22	5.3-10.6	3
b)	21x0.8x0.8	50	-24	5.86-11.72	4
c)	30x6xN/A	19	-28	2.9-5.8	2
d)	30x1x0.5	3	-20.97	9.41-18.82	5

Table 4.3: Features of different tag realizations with CE values recorded for an incident power of -15 dBm

From Fig. 3.7b, we initially observe CE of approximately -40 dBi. However, with the introduction of new designs, significant optimizations are evident. For example, for configuration c) in Table 4.3, operating at the same frequency as the curve from Fig. 3.7b, shows an improvement of up to 12 dB by using a different tag design.

4.2 Diode Model

Having selected the diodes of interest, we first conduct performance simulations using the ADS software. For this, we input the characteristics of the diodes into predefined models as prensented in Table 4.4, with parameters sourced from the datasheet provided on the merchant's website.

Parameters	SMS7630-040LF	SMS7621-040LF	Description
C_{j0} [pF]	0.14	0.1	Zeros Bias nonlinear junction capacitance
I_s [A]	5E-6	4E-8	Saturation current
R_s [Ω]	20	12	Ohmic resistance
N [–]	1.05	1.05	Emission coefficient
V_j [V]	0.34	0.51	Contact potential
M [–]	0.40	0.35	Grading coefficient
TT [sec]	1E-11	1E-11	Forward transit time
E_G [eV]	0.69	0.69	Energy gap
XTI [–]	2	2	Saturation current temperature
F_C [–]	0.5	0.5	Forward-bias depletion capacitance coef.
B_V [V]	2	3	Reverse breakdown voltage
I_{BV} [A]	1E-4	1E-5	Current at breakdown voltage

Table 4.4: SPICE model of the selected diode

The purpose of conducting simulations is to accurately predict the performance of the component. It is therefore crucial to ensure that these simulations align with the actual performance observed in real-world conditions before integrating the component into a more complex system. With this objective in mind, we compare the I-V curves from the ADS simulation with the actual curves obtained from large-signal measurements.

To obtain the ADS simulation curves, the following scheme in Fig. 4.3 is used.

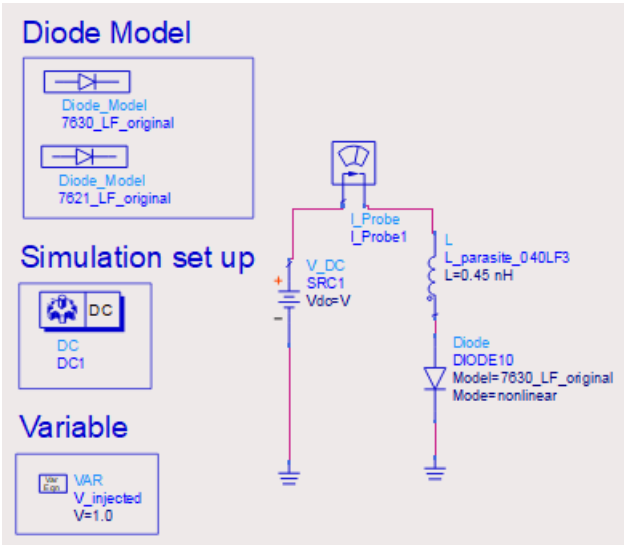

Figure 4.3: The simulation is run in DC mode, varying the source power from 0.1 to 0.7V, aligning with the power range specified in the datasheet.

As for the experimental curves, measurements are carried out using an SMU 2450 according to the layout shown in Fig. 4.4.

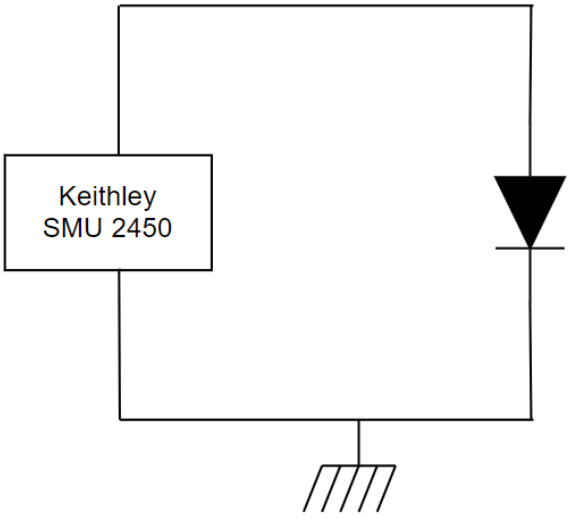

Figure 4.4: Scheme of the circuit for measuring IV curves

Knowing that the circuit contains parasitic resistances, notably due to the presence of cables, a measurement of this has also been performed and then deduced from the measurements initially taken in order to obtain the most accurate measurements. It is challenging for two electronic components of the same type to exhibit identical electronic properties due to inevitable variations in the manufacturing process. As a result, their performance characteristics may not be exactly the same but could show slight differences. To determine the general behavior of the diode, we have conducted experiments on three diodes of the same class.

Now that we have the different curves, we obtain the graph shown in Fig 4.5.

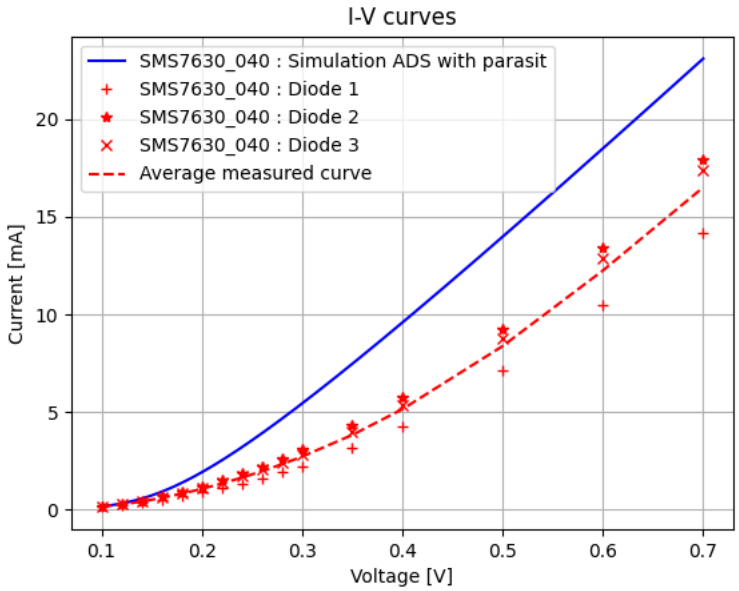

Figure 4.5: We measure the current flowing in the circuit when applying different voltages in the interval 0.1V-0.7V.

The observed difference between diode behavior in simulation and reality indicates a need to adjust the SPICE model parameters to match the experimental data. Thus the updated parameters are detailed in Table 4.5.

Col1	SMS7630		SMS7621	
	Previous	Updated	Previous	Updated
N [–]	1.05	1.1	1.05	1.05
I_s [A]	5e-06	1.3e-06	4e-08	4.4e-08
R_s [Ω]	20	25	12	9
B_V [V]	2	0	3	0

Table 4.5: Parameters that affect the performance of large-signal before and after fitting the curves

The results are shown in Fig. 4.6. We observe that the simulation curve has closely aligned with the average measured curve, though it still exhibits some minor differences across all voltage levels.

Next, we determine the power interval of interest, given the fixed power emitted by the transmitting antenna. As previously defined, the EIRP must be multiplied by the effective area of the tag's receiving antenna, corresponding to a loss of approximately -30dBi. We neglect the effect of distance-related losses, assuming the maximum power injected into the tag is 10dBm. Base on data from Fig. 3.7, we limit our low-power calculations to -26dBm, as the sum of the tag's output power and path loss approaches ambient noise levels. Thus, simulations are conducted within the power range [-26dBm:10dBm].

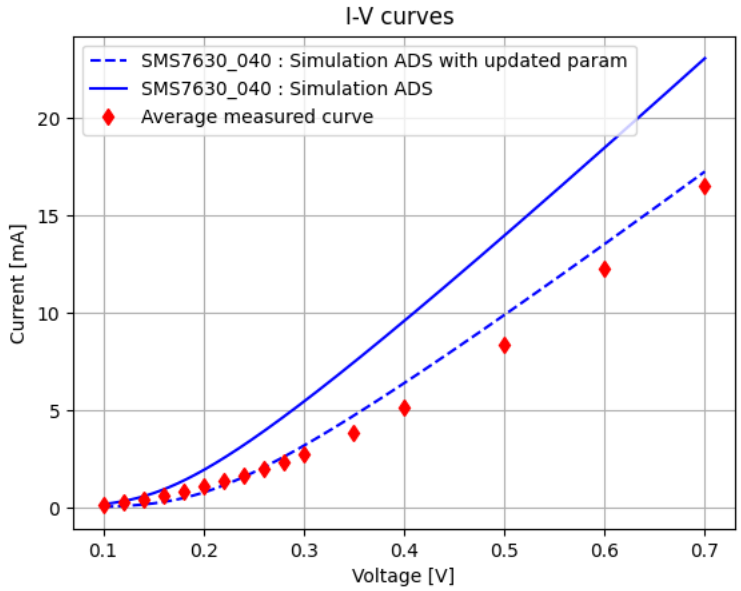

Figure 4.6: Measurement of the current flowing in the circuit when applying different voltages in the interval [0.1:0.7]V

4.3 Circuit Design

The circuit shown in Fig. 4.1 can be viewed as in Fig. 4.7.

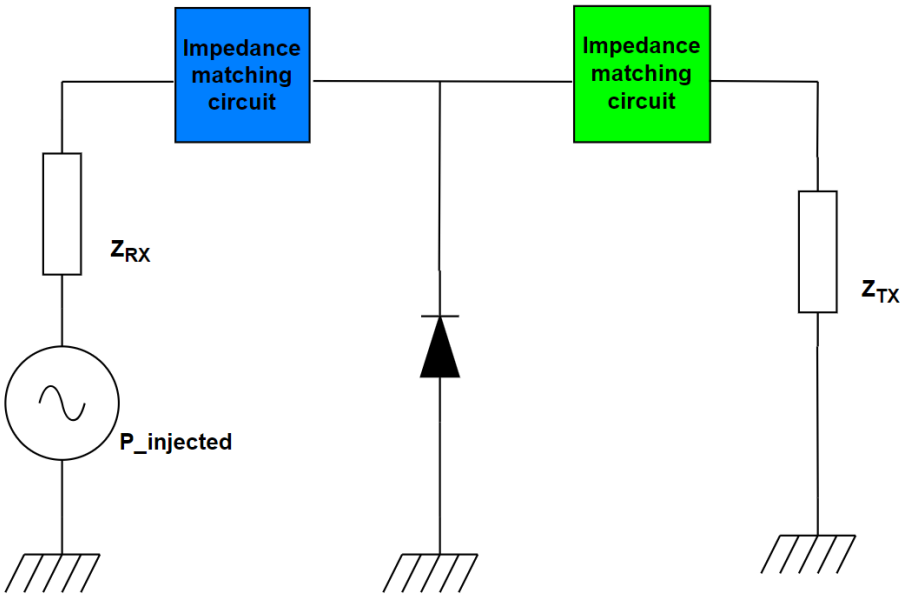

Figure 4.7: Circuit Tag representation : The voltage source represents the power picked up by the receiving antenna and injected into the circuit. The impedances represent the different antennas.

With this setup, we evaluate the best performance our diodes can achieve to understand the upper performance limit. To do this, we define various concepts and tools that are used later. First, the blue (left-hand side of the circuit) and green (right-hand side of the circuit) blocks are ideal components representing different

impedances at different frequencies.

At the fundamental frequency, the blue block acts as a wire with zero impedance, while the green block acts as an open circuit to prevent the signal from reaching the right part of the circuit. At the harmonic frequency, the opposite effect occurs: the blue block becomes a short circuit, and the green block becomes a closed circuit, allowing the harmonic signal to propagate to Z_{TX}. For maximum power transfer, the diode impedance at 2.9GHz should match the conjugate of the antenna impedance Z_{RX}, and similarly at 5.8GHz for Z_{TX}.[8]. The power formula is defined as:

$$P = 0.5(VI^*) \tag{4.1}$$

where V and I are complex elements across the diode.

We use various tools in ADS, such as Harmonic Balance and the optimizer, to achieve the desired performance. HB simulation enables frequency-domain analysis technique for obtaining the steady-state solution of nonlinear circuits and systems. This allows us to analyze nonlinear electrical circuits with nonlinear differential equations and find a solution.[39]

The optimizer tool in ADS automates the process of achieving the desired circuit performance by modifying circuit component values to meet specific optimization goals. The tool employs different search algorithms, including random search, gradient search, and a hybrid method combining both. According to the document, the random method often approaches the global solution, while the gradient method may lead to local solutions. Hence, the hybrid method is preferred for more reliably reaching the global solution. We aim to maximize output power at the harmonic frequency, defined as max (Conversion) =max $\frac{P_{output}}{P_{input}}$ =max $(\frac{0.5(V_{output}I^*_{output})}{0.5(V_{input}I^*_{input})})$.

The resulting circuit is shown in Fig 4.8. One thing to note is that the diode impedance depends on the current, which in turn depends on the power it receives, and this in turn depends on the range.[37]. To find the performance limit, we optimize the circuit for different power levels, resulting in different impedance values (Z_{RX}, Z_{TX}). This yields a range of impedance values, each providing maximum power conversion.

Now, let's examine the performance limits of the diodes, as shown in Fig. 4.9. At all power levels, losses are inevitable, as perfect conversion is not possible. A general trend for diode 7630 shows greater losses at lower power levels, reaching up to -11dBm at -26dBm, but as power increases, these losses decrease accordingly. The diode 7621 exhibits less conversion loss primarily due to its lower series resistance. However, above -5dBm, the performance deteriorates significantly. This decline could be attributed to two possible factors. The first is likely related to a simulator issue. The second concerns its design, as a Schottky diode which operates optimally within a specific power range, it may have exceeded this interval. Consequently, from the upper limit performance view, the 7630 diode is preferred for its stable performance over the entire range of interest.

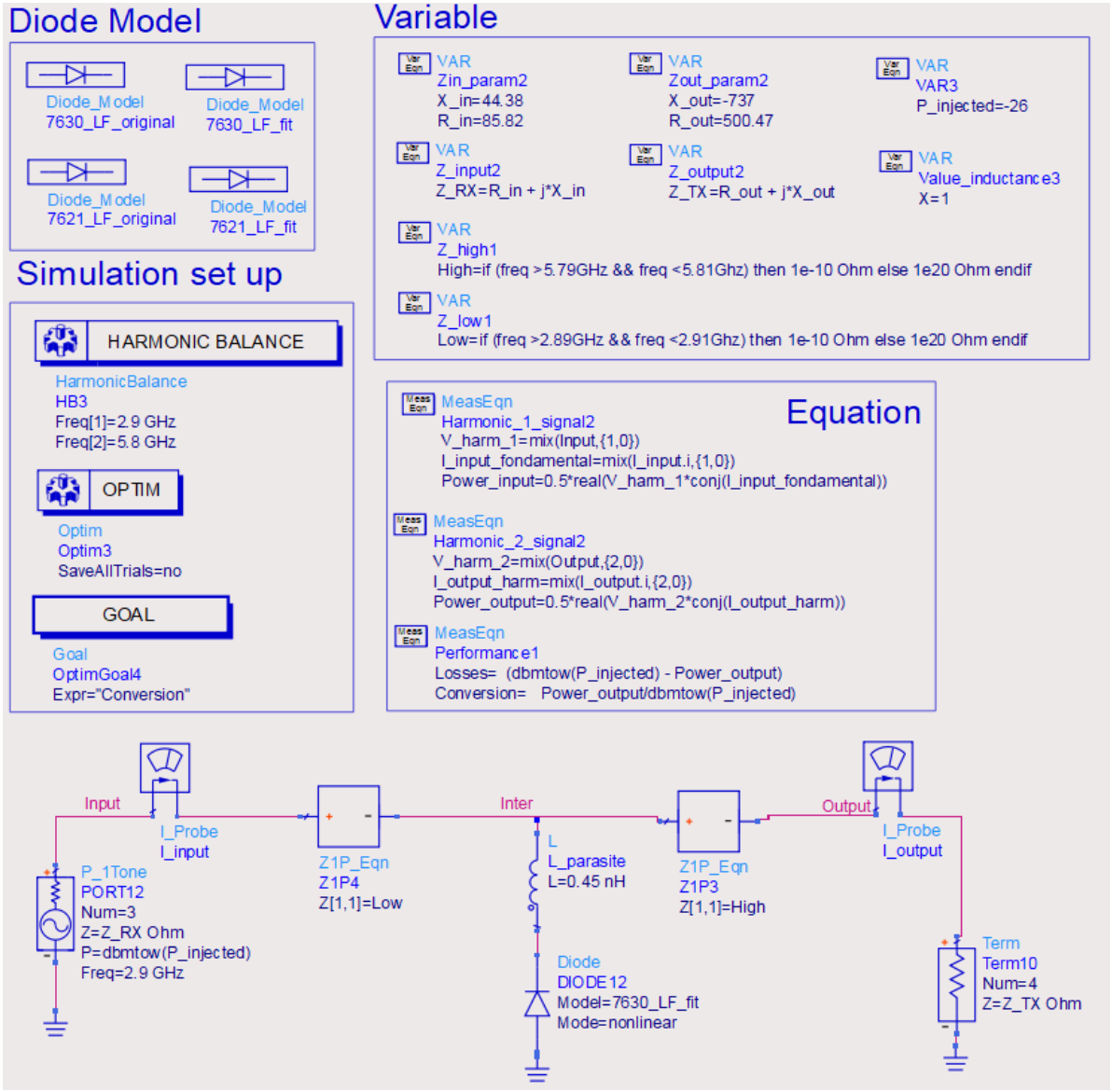

Figure 4.8: ADS circuit for simulating the best performance of the diode

The impedance evolution as a function of power is also noteworthy and is shown in Fig 4.10, with normalized data (normalization of 500) for clarity. At the fundamental frequency, the real part of the diode's impedance varies slightly, with a difference of 0.4 for a power difference of 36 dBm. In contrast, the reactive part varies significantly, ranging from 0.8 to 5.1 in the scale of 500 over the studied power interval. Thus, at 2.9 GHz, the reactive part of the diode's impedance is more sensitive than the real part. For Z_{TX} at the harmonic frequency, both parts of the diode's impedance are equally affected by variations in input power.

4.3.1 Worst case design

Since it is impractical to create equipment capable of adjusting the impedance values based on the input signal power on the tag under various constraints, we must use fixed impedances. The diode behavior varies according to these fixed impedance

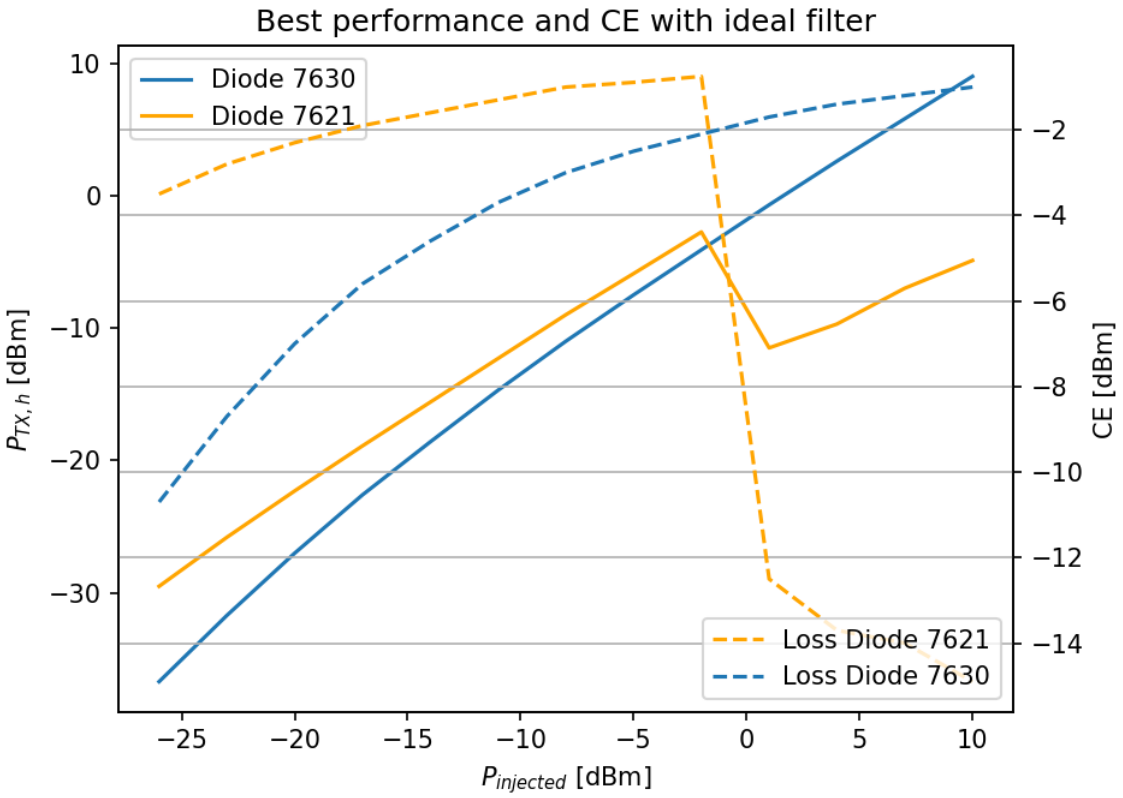

Figure 4.9: Best performance (left-hand y-axis and solid lines) and CE (right-hand y-axis and dashed lines) of the selected diodes

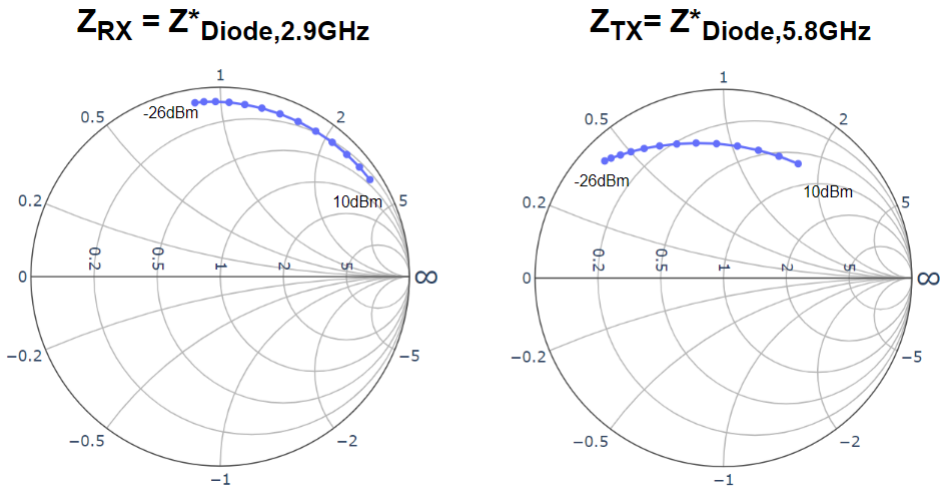

Figure 4.10: Evolution of impedance over the incident power level from -26 dBm to 10 dBm by step of 3 with the use of diode 7630

values. To better understand performance trends at different power levels, we divide the power range into three parts. For each part, we use the impedance pair optimized for a specific power level within that range to observe its performance over the studied power interval. The results are shown in Fig 4.11.

Fig. 4.12 illustrates the corresponding losses of the curves in Fig. 4.11.

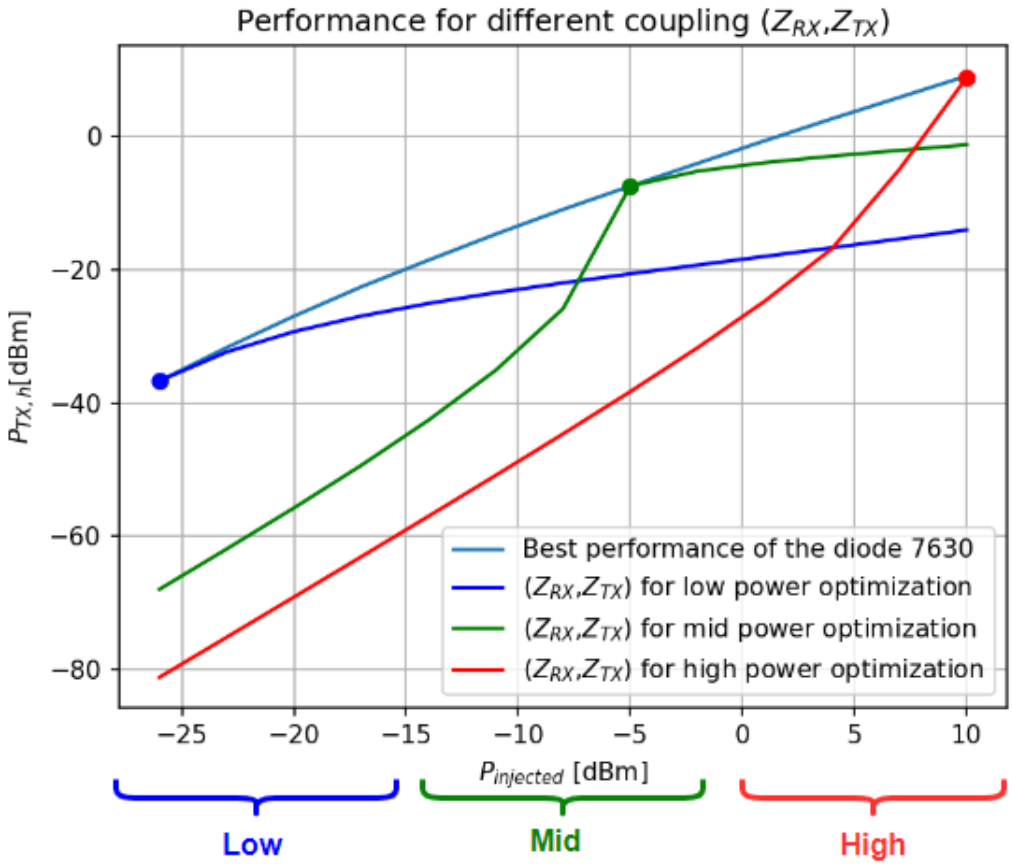

Figure 4.11: Evaluation of output power by using the best couple of impedance (Z_{RX}, Z_{TX}) for each power incident level with the use of diode 7630

We can observe that the performance differs significantly based on the impedance pair used. When using the impedance pair optimized for low power, losses are the lowest at weak power and then increase with significant value at high power. For the second case, losses are substantial at both low and high power. Finally, for the third case, losses are also significant in the other two scenarios. As previously explained, the power injected into the tag corresponds to the EIRP minus the path loss. Hence, when the tag receives high power, it indicates proximity to the transmitting antenna, and as the distance increases, the incident power on the tag decreases.

	Low	Mid	High
CE	★☆☆	★★☆	★★★
Path Loss	★★★	★★☆	★☆☆

Table 4.6: Optimized (Z_{RX}, Z_{TX}) for the incident power level -26dBm

Therefore, we ask ourselves which impedance pair best fits our application. One possible approach is to design for the worst-case scenario. The principle of worst-case design involves optimizing for the most challenging situation to ensure the system performs adequately under all conditions. By optimizing for the worst case, we intuitively know that more favorable situations will still exhibit better performance.

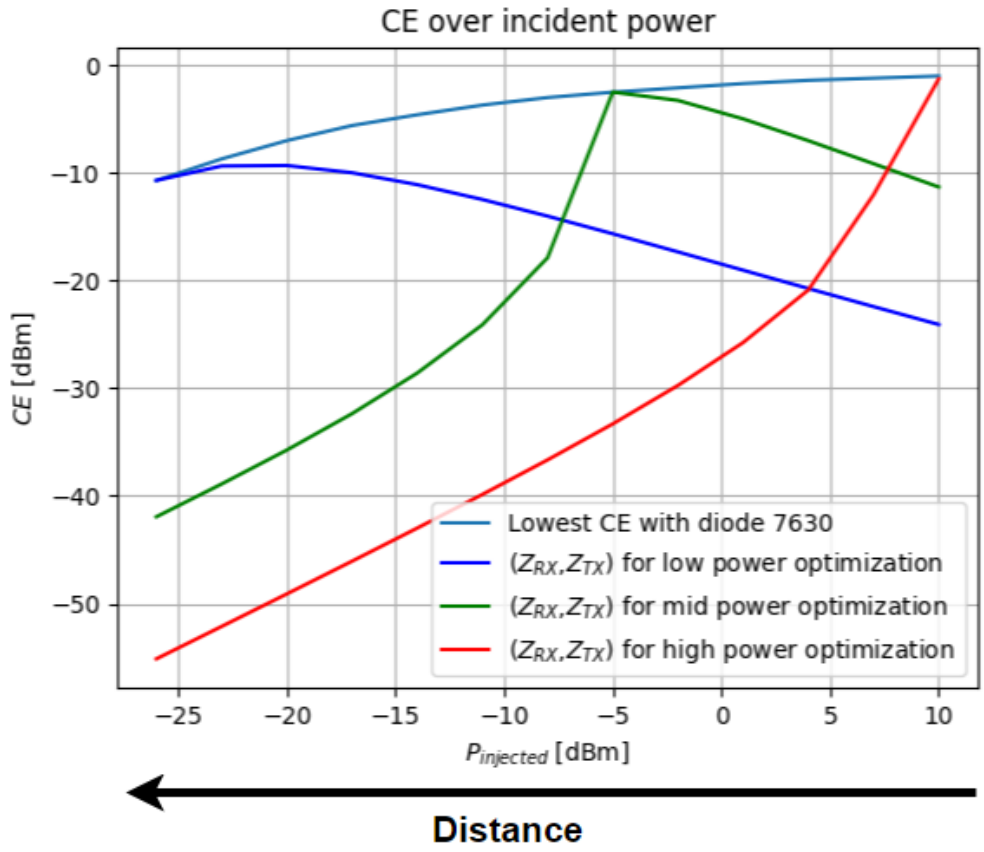

Figure 4.12: Evaluation of CE corresponding to Fig. 4.11

	Low	Mid	High
CE	★★★	★☆☆	★★☆
Path Loss	★★★	★★☆	★☆☆

Table 4.7: Optimized (Z_{RX}, Z_{TX}) for the incident power level -5dBm

In our detection system, with the assumption that tag performance remains constant, the goal is to maximize the detection range. The worst-case scenario is defined by the longest distance where the system remains functional. In this context, the worst-case scenario for the tag is when it receives the minimum power while still maintaining functionality. From Fig 4.11, we observe that the worst-case is defined for low power levels because, with a fixed transmitted power, low received power indicates a large distance.

We verify that optimizing for low power levels ensures acceptable performance at other power levels, meaning the system remains functional. Observing Table 4.6,4.7,4.8, losses associated at lower power levels can be compensated with distance-related losses, which is not the case if we optimized for other power levels.

Therefore, we optimize the circuit for low power levels.

	Low	Mid	High
CE	★★★	★★★	★★☆
Path Loss	★★★	★★☆	★☆☆

Table 4.8: Optimized (Z_{RX}, Z_{TX}) for the incident power level 10dBm

4.3.2 Antenna Impedance

Next, we define the antenna impedances, which are calculated based on the use of dipole antennas, a common configuration in this field. However, it is worth noting that other types of antennas could also be employed depending on the specific application requirements. The impedance values are determined using a MATLAB script developed by Professor Craeye, which simulates the impedances for these antenna configurations, based on some parameters such as number of basis functions used in calculation, the wire radius and length of the antenna. In our application, to achieve the lightest possible tag, we opted for the thinnest copper wire available, with a radius of 0.13mm. The antenna length is determined by half the wavelength at 2.9GHz, which is 5.2cm. The impedance curves resulting from these parameters are presented in Fig. 4.13.

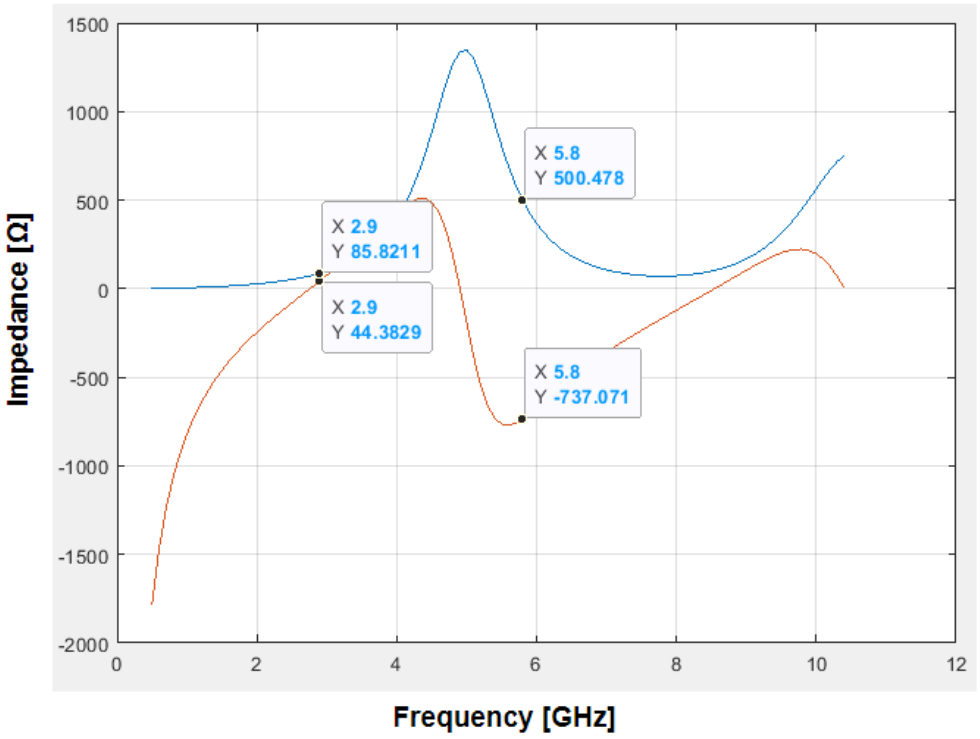

Figure 4.13: Variation of impedance of dipole antenna of length 5.2cm over frequency. The blue curve corresponds to the real part of the impedance, while the orange curve represents the imaginary part. The selected impedance values are highlighted.

We then examine the impact of this couple of impedance on the performance. The impedance values of the circuit represented in Fig. 4.8 are replaced by those shown in Fig. 4.13. We maintained the same configuration, with two ideal blocks,

because physically, there is only one dipole antenna operating at two frequencies. As a result, the circuit cannot simultaneously handle two distinct impedances, necessitating the use of ideal components to separate them effectively. The resulting performance is shown in Fig. 4.14.

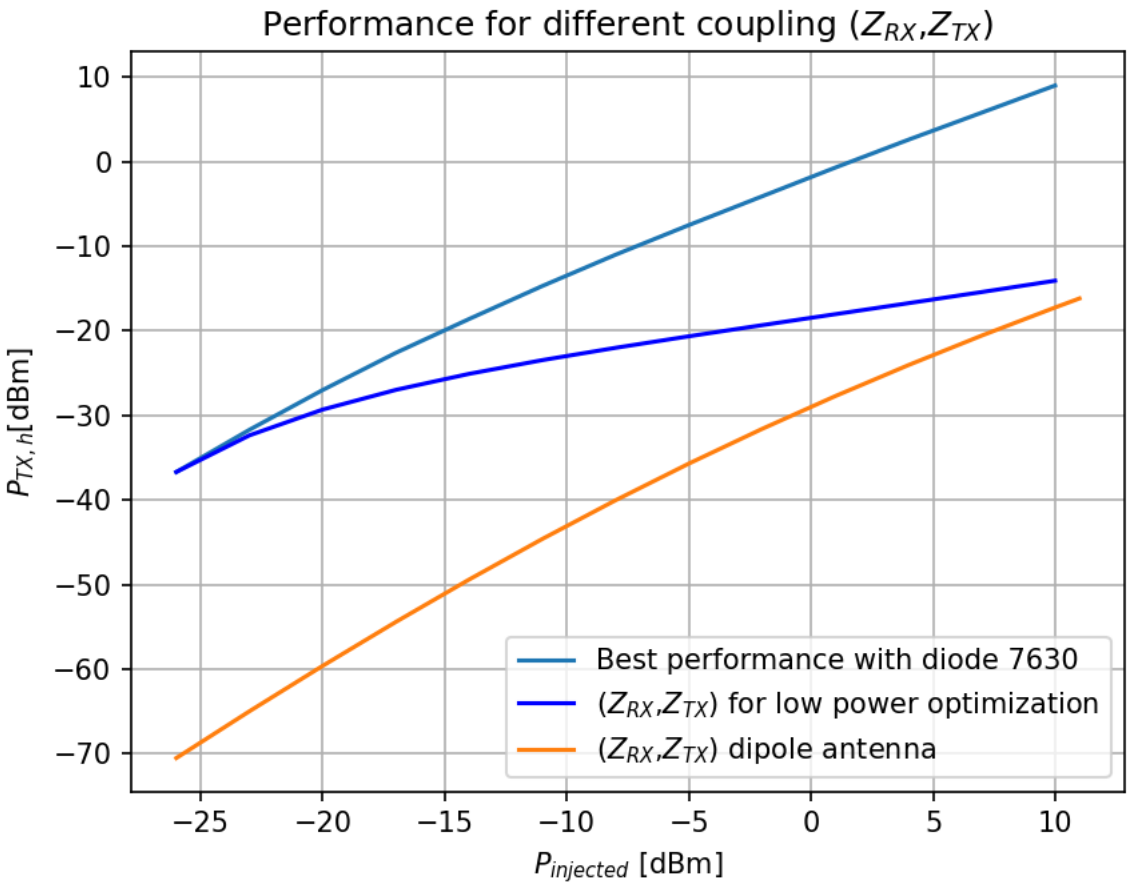

Figure 4.14: Evaluation of output power with Diode 7630 by using the different couple of impedance (Z_{RX}, Z_{TX})

We observe significant performance degradation at low power levels, with approximately -35 dBm of loss at an incident power level of -26 dBm. However, this degradation decreases as the power increases. Since we aim to improve the worst-case scenario, these results are not acceptable, and we must find a way to enhance the performance. From the state of the art, we know that adding an inductance would rise the performance. We aim to quantitatively investigate the improvements provided. Therefore, we add an inductance in parallel with the diode in the ADS circuit. Since this inductance is not perfect, it includes a parasitic resistance that is also introduced into the circuit. The resulting circuit is shown in Fig. 4.15.

Next, following the worst-case design method, we optimize the inductance value to achieve the highest output power at -26dBm. The resulting performance is shown in Fig. 4.16.

This confirms the findings in the literature: adding an inductance indeed improves the system's performance. Improvements are primarily observed in the

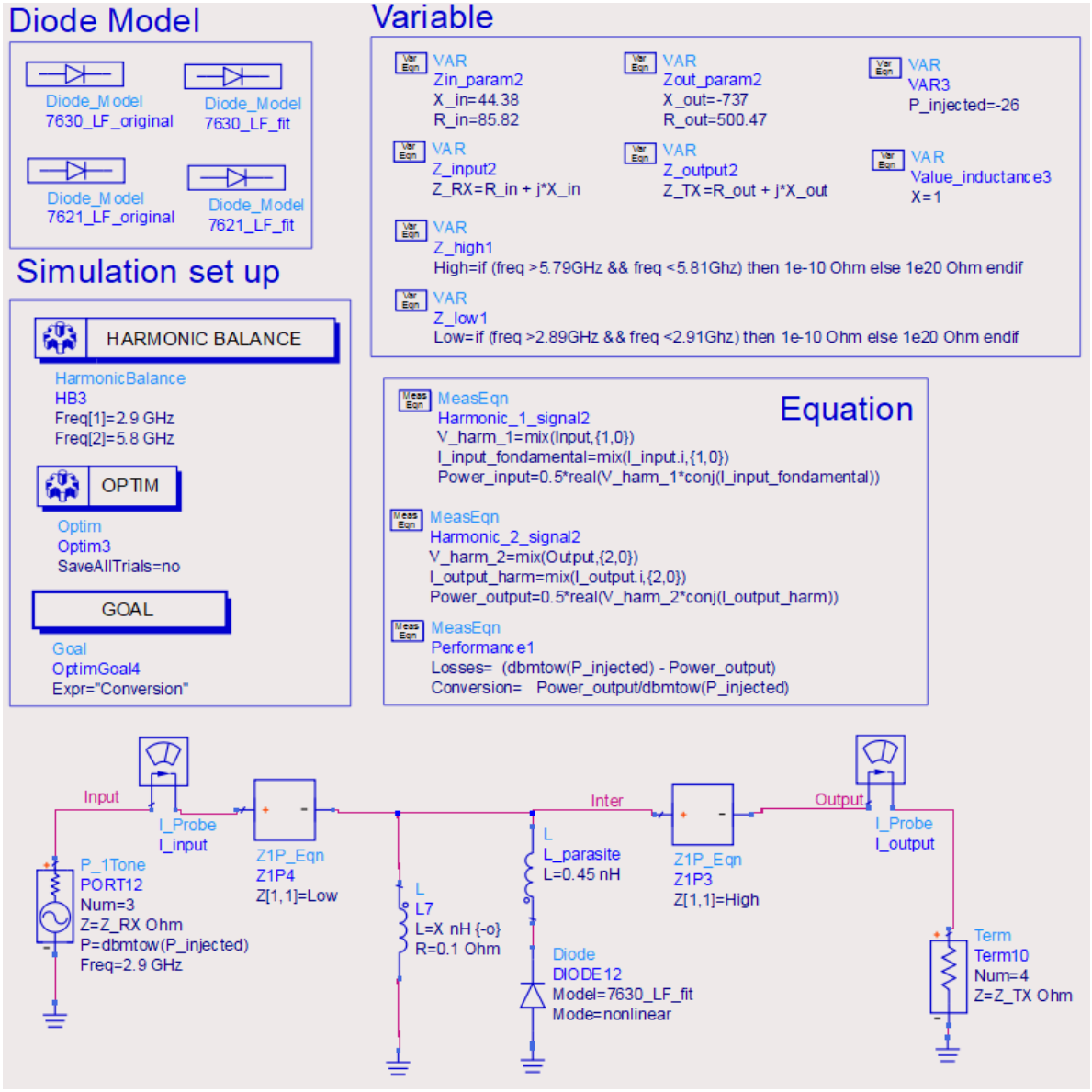

Figure 4.15: ADS circuit for simulating the tag using dipole antenna

medium and high power ranges, while at lower power levels, the gain is relatively modest. Nevertheless, even at low power, there is a notable benefit from the simple addition of an inductance.

Moreover, this inductance is easy to implement and integrate into the design by using a simple wire loop, with the inductance value calculated using the formula provided in 4.2.

$$L = \frac{\mu_0 \mu D}{2}[ln(\frac{8D}{d}) - 2] \tag{4.2}$$

- D is the diameter of the loop
- d represents the diameter of the wire

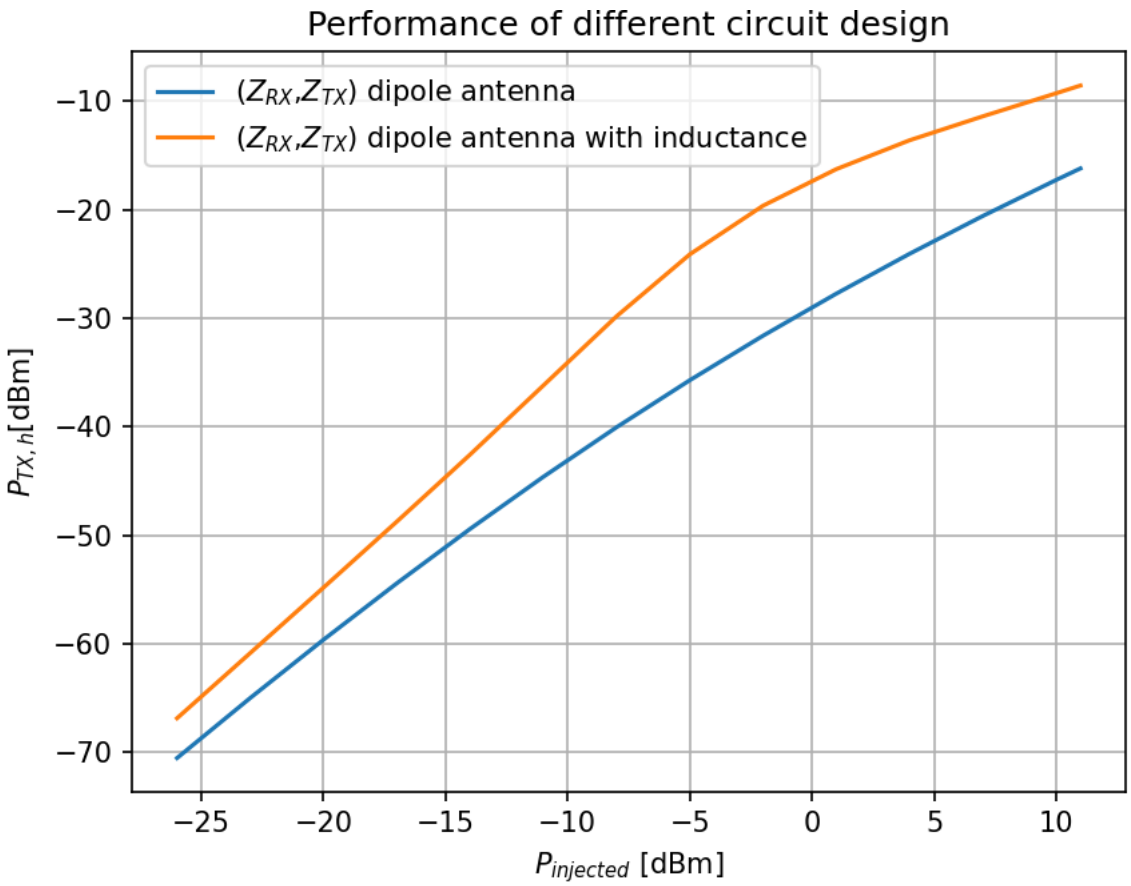

Figure 4.16: Evaluation of output power with Diode 7630 by using the couple of impedance (Z_{RX}, Z_{TX}) found for dipole antenna without/with inductance of 4.8 nH

This approach aligns with the design shown in Fig. 4.2d.Subsequently, we can compare these performances with those documented in the literature.

It is also valuable to compare the performance of the two diodes to provide an initial evaluation within a specific design, here the dipole antennas. The performance results are presented in Fig. 4.17.

We can observe that the diode 7630 generally offers better performance, although the difference is minimal. Then, with this updated power conversion curve, we can revise the link budget and analyze the resulting improvements, as shown in Fig. 4.18.

At a distance of approximately 12m, we observe a gain of 15dBm in the power received by the antenna. Given that the signal strength is well above the noise level, we are now interested in determining the new maximum detection distance achievable under these conditions. This is shown in Fig. 4.19.

Unfortunately, as we are limited to a power range, we lack information about the conversion loss for incident power below -26dBm. This constraint limits us to a distance of 16m, but we can see that this is not the system's limit. Based on the curve trend, we could approximately reach a distance of 18m, which is 1.5 times the

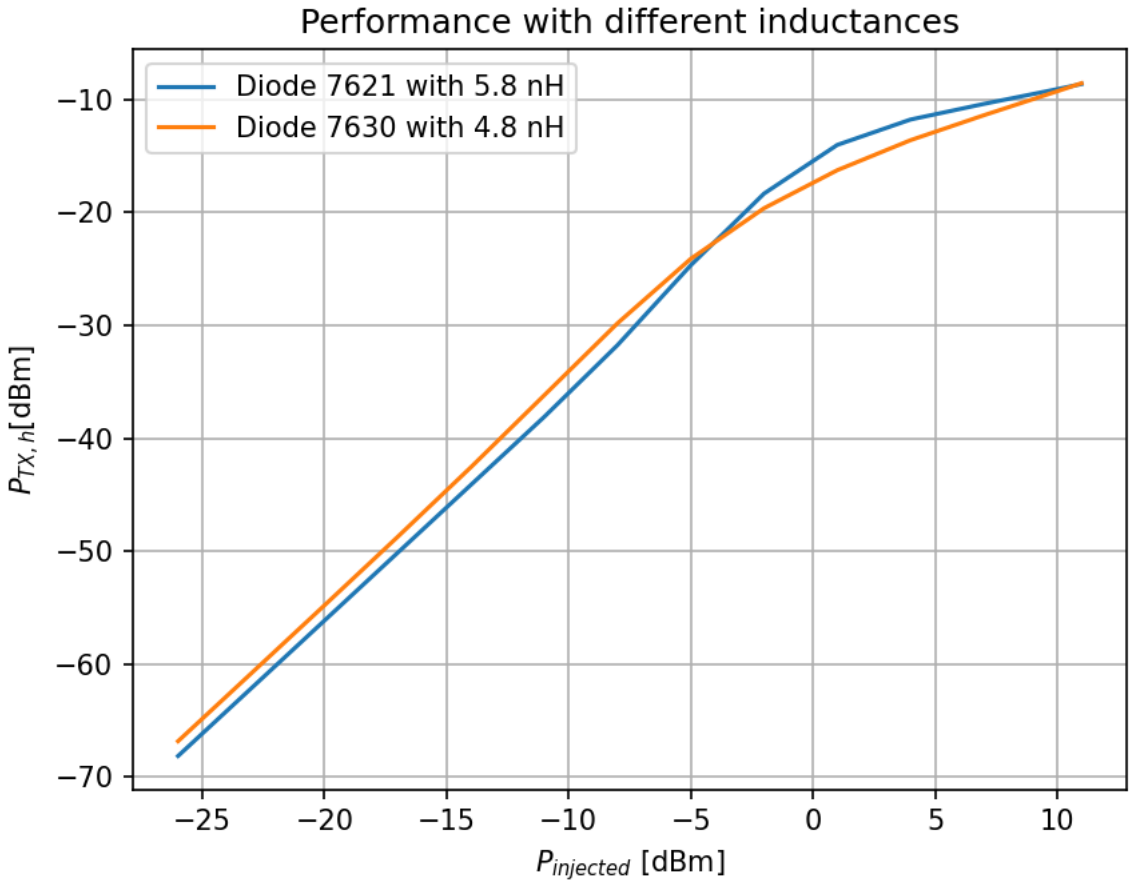

Figure 4.17: Evaluation of CE over the range of power

initial distance.

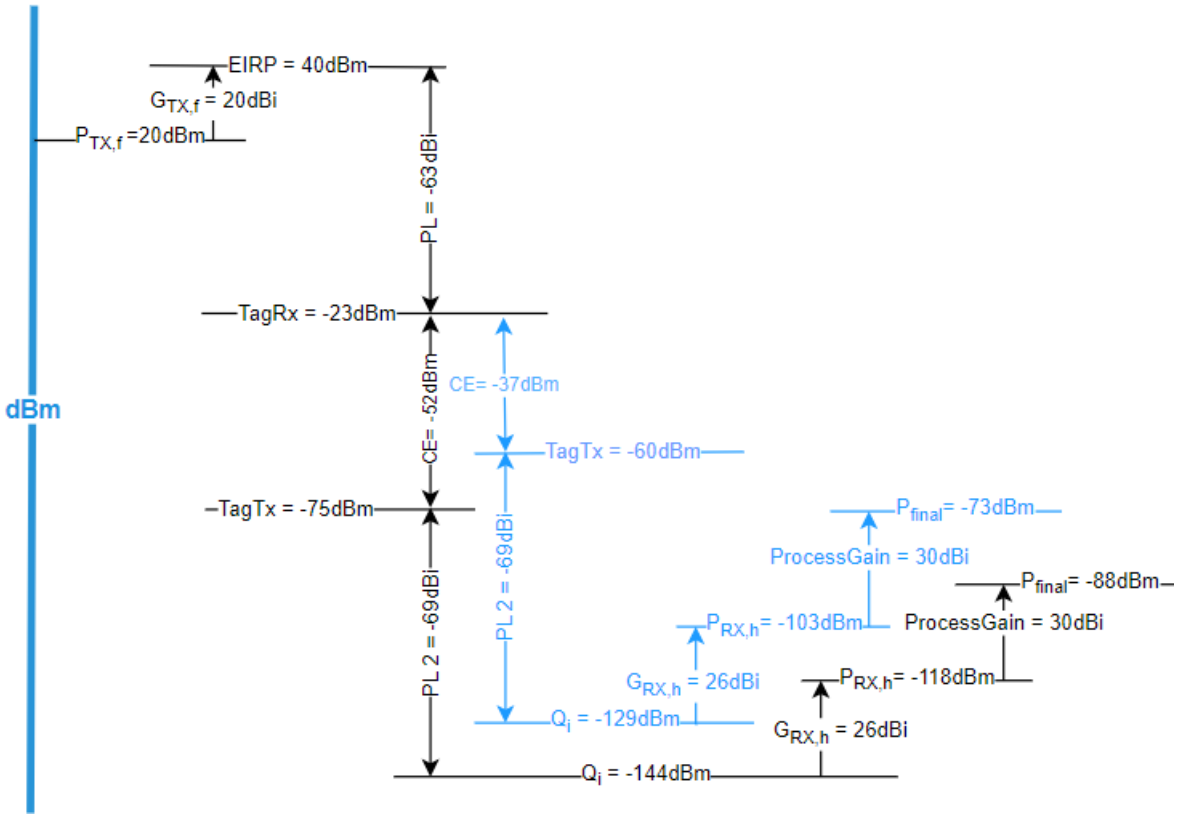

Figure 4.18: Comparison of the previous link budget (dark arrows) and the one with new tag (blue arrows) for a distance of 12m

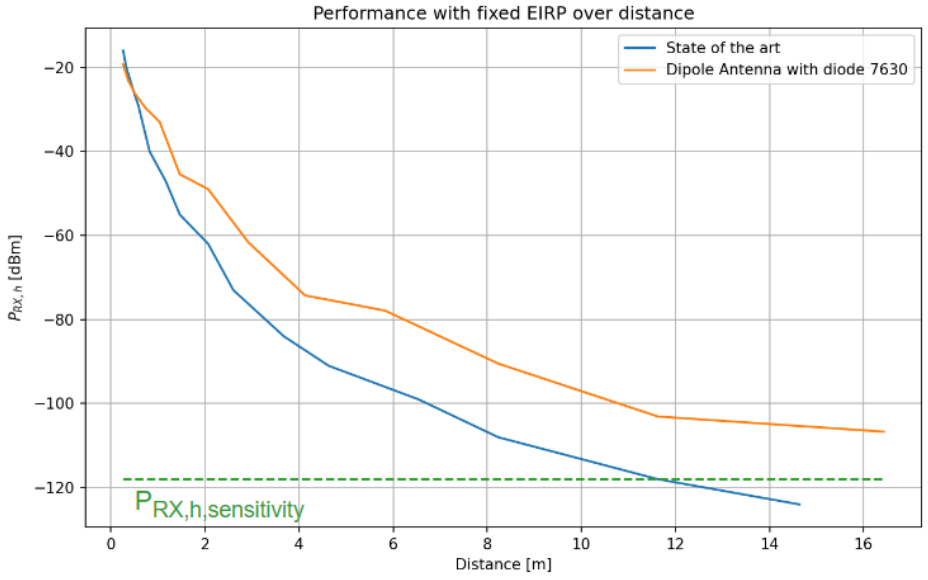

Figure 4.19: Received power over the distance using two different tags, one from

Chapter 5

Experimental data

We now turn our attention to the reliability of these simulations. To validate our results, one possibility is to conduct an antenna experiment designed to measure the tag's performance. Before proceeding, we need to carefully select the tags to be tested.

5.1 Tested tag

Building on the design from Fig. 3.2a, the values of the electrical components must be optimized to achieve the best possible performance. Fig 5.1 illustrates the variation in output power at the harmonic frequency as the inductance value is adjusted, with an incident power of -26dBm.

We observe that with the use of the 7630 diode, optimal performance is achieved around 5nH. However, it is also evident that beyond 10nH, further increases in inductance do not result in significant performance losses. Therefore, we aim to limit the inductance to more practical values, neither too high nor too low, while still maintaining acceptable performance. The final inductance value selected is 10.6nH. Since the tag loop represents the inductance, it is crucial to ensure that the loop achieves the desired value. To do this, the inductance is determined using 4.2.

Since the goal is to make the tag as small and lightweight as possible, we use 0.26mm diameter copper wire. Consequently, the tags to be tested have been fabricated according to the specifications listed in Table 5.1.

	μ_0	μ	D [mm]	d [mm]	L [nH]	Weight[mg]	Dimension [mm]
SMS7630	$4\pi 10^7$	1	5.2	0.26	10.6	32	52x5.2x1
SMS7621	$4\pi 10^7$	1	5.2	0.26	10.6	32	52x5.2x1

Table 5.1: Characteristics of the tested tags

The results obtained with this tag configuration are presented in Fig. 5.2.

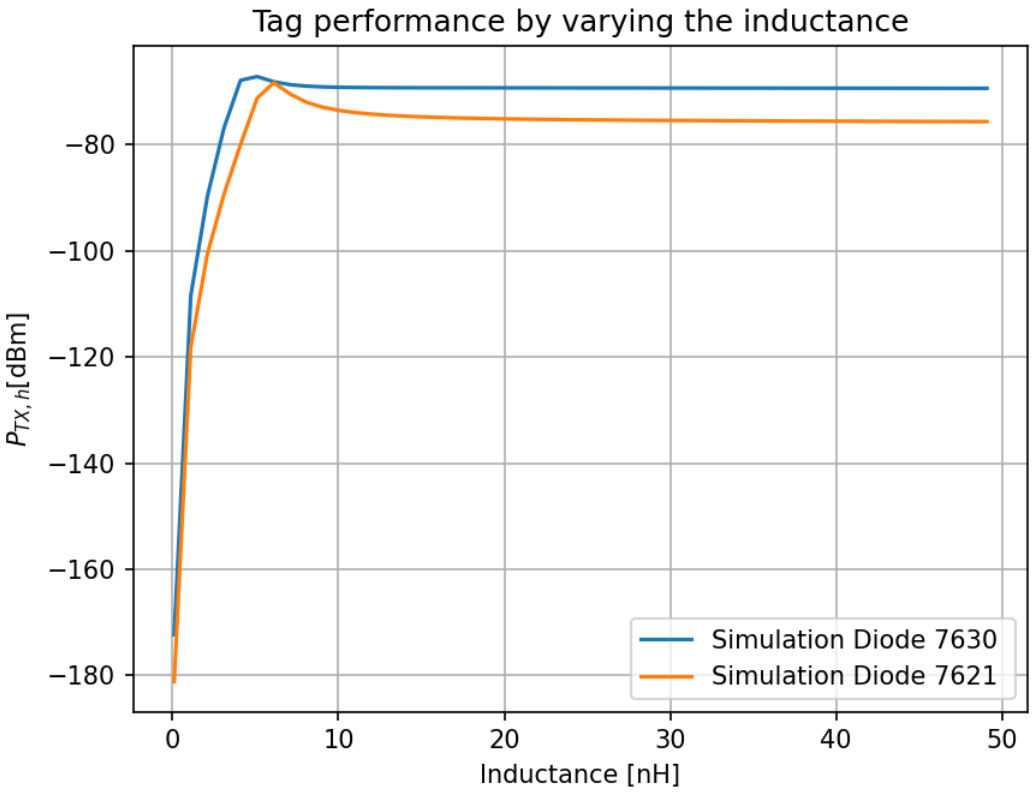

Figure 5.1: Evaluation of performance by varying the inductance

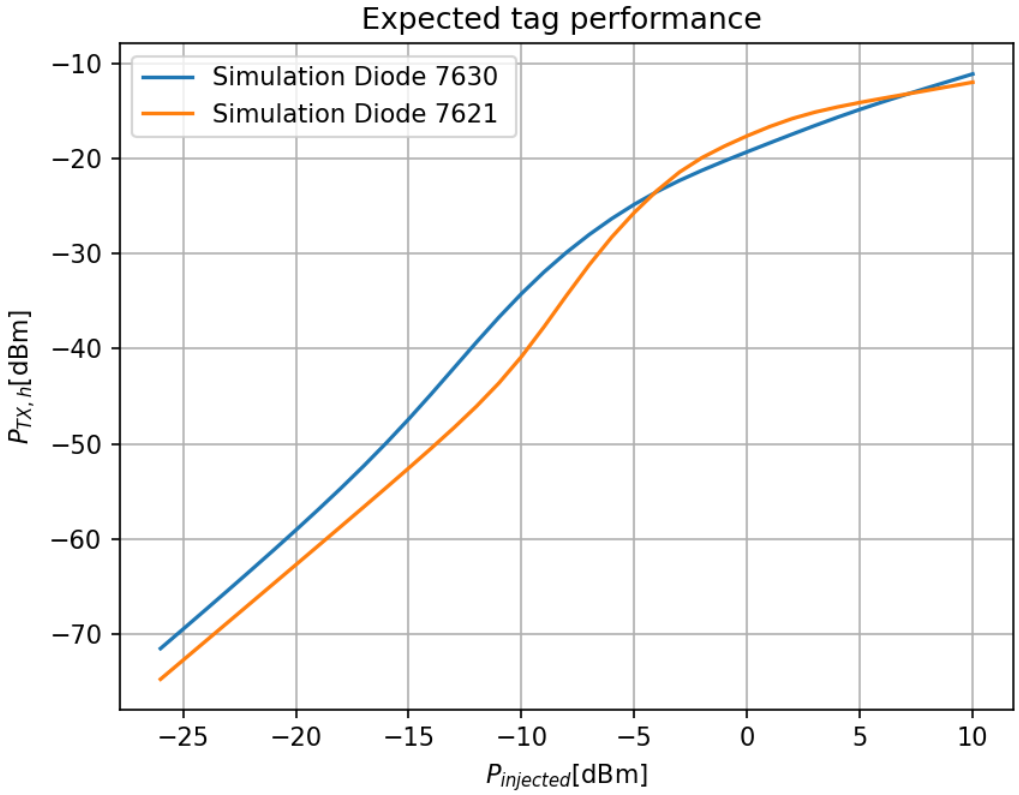

Figure 5.2: Expected performance for the tested tags

5.2 Set up

To evaluate the performance of our tag, we will conduct an antenna experiment, as it is challenging to directly measure the tag's output power. The principle of this experiment is illustrated in Fig. 5.4.

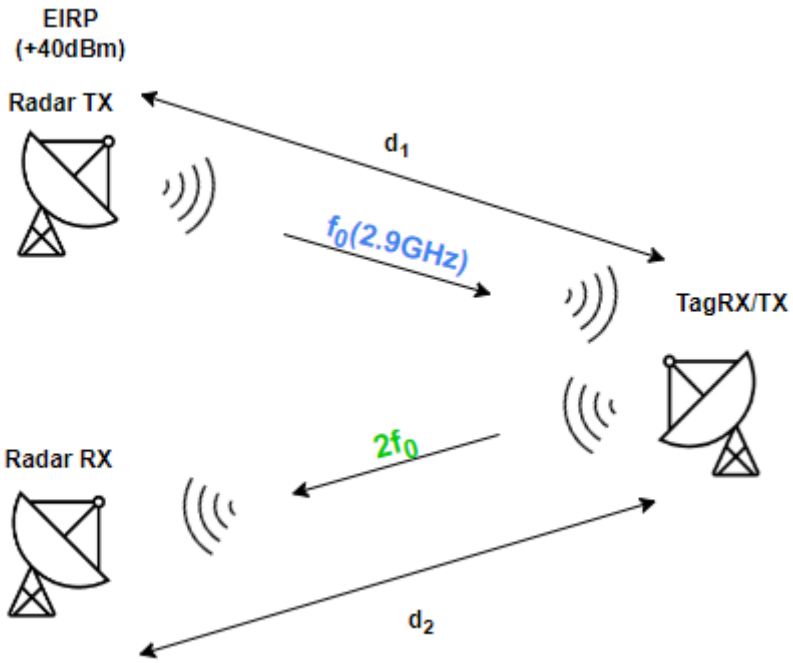

Figure 5.3: Antenna Experience

By analyzing the measurements taken at the Radar TX and RX antennas, along with knowledge of signal losses due to distance,we can determine the power conversion at the tag.

Specifically, to carry out this experiment, we will follow the setup plan shown in Fig. 5.4 with the various components explained in detail throughout the rest of this chapter.

VNA stands for "Vector Network Analyzer" and is used in RF domains to measure the frequency responses of active or passive components and networks. The measurement principle involves sending a signal to the Device Under Test (DUT) and analyzing the received response. The VNA allows for the measurement of both phase and amplitude of electronic components across different frequencies [12]. For our experiment, we use the VNA model PNA-X N5242B 26.5GHz with 4 ports. It is capable of transmitting a signal at 2.9GHz and measuring the received signal at 5.8GHz.

PA stands for "Power amplifier" and boosts a low-power signal to a higher power level. Since the VNA cannot deliver power higher than 10dBm, we use a PA capable of providing a gain of 34dBm, reaching saturation at that point. However, during the system integration, the PA performance was capped at 30dBm.

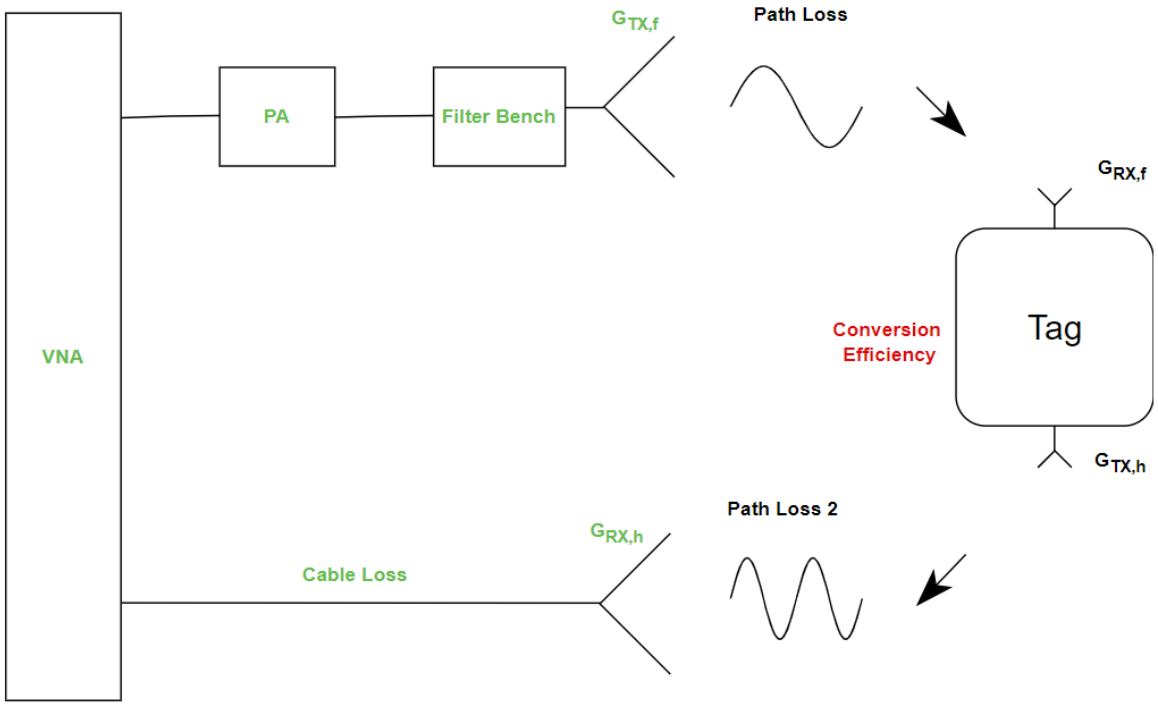

Figure 5.4: Overall experimental setup to evaluate tag performance. The green text indicates known parameters, while the red text represents the target performance metrics to be measured.

The PA exhibits non-linear behavior, leading to the unwanted generation of harmonics. To prevent these harmonics from being transmitted through the transmission antenna, a filter bank is used to attenuate frequencies above 3GHz.The VNA can configure the power present after the filter bench, with a range varying from -5dBm to 30dBm.

The signal received by the receiving antenna must pass through a bandpass filter via a long cable to ensure that only the harmonic component is delivered to the VNA. During this transmission, signal losses are inevitable and are illustrated in Fig. 5.5. We observe that the cables exhibit losses of up to -8dB at the harmonic frequency.

The transmission antenna used is the R&S HL024A1, which has a characteristic gain of 6dBi. The receiving antenna is the R&S HL025, covering a frequency range of 1GHz-26GHz, with a characteristic gain of 8dBi.

The powers received by and then re-radiated by the harmonic transponder in decibels are given by 5.1 and 5.2 where L_c represents the cable loss.

$$P_{\text{injected}} = EIRP - \text{PathLoss}_f + G_{TagRX} \tag{5.1}$$

$$P_{output} = P_{Received,VNA} + L_c - G_{RX} + \text{PathLoss}_h - G_{TagTX} \tag{5.2}$$

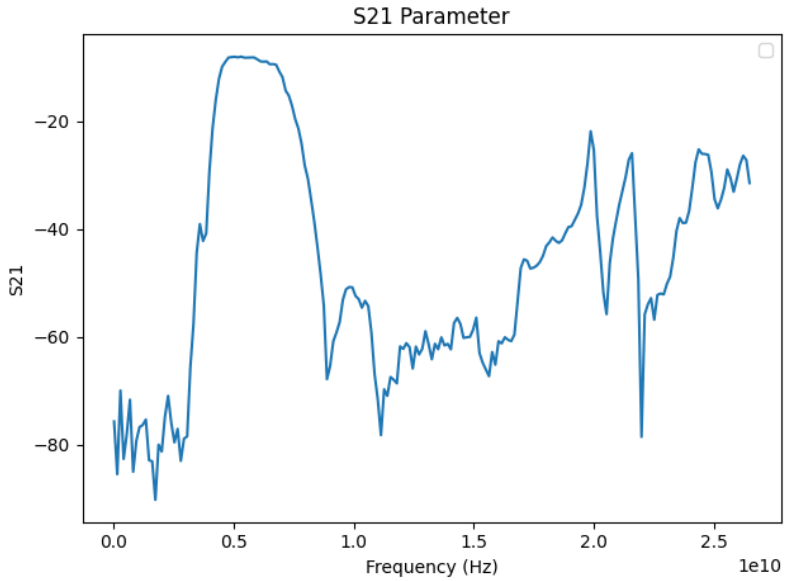

Figure 5.5: S21 parameters between the receiving antenna and the VNA

5.3 Measurement

Using VNA measurements, we can perform reverse engineering to determine the power injected into and emitted from the tag. However, before proceeding, we need to establish certain assumptions:

- Path loss model : Free Space Path Loss (FSPL)
- Antenna gain : 2.15dBi and 2.55dBi
- Radiation pattern : As illustrated in Fig. 5.7

5.3.1 Path loss

The FSPL model is applied under specific conditions, particularly in the far field of the antenna, with no obstacles between the transmitter and receiver. To verify the first assumption, we positioned the antennas facing each other at various distances, ensuring a clear line of sight, and measured the transmitted and received power levels. According to **??**, the threshold for the far field is 0.67m. The performance data are presented in Fig. 5.6.

The results show that when operating in the near field (0.23m), the FSPL model deviates from predictions by approximately 4 dB. In contrast, in the far field, the deviations reduce to just 1 to 1.25dBi, confirming our initial hypothesis.

The second assumption, related to antenna gain, is challenging to verify directly due to the difficulty of determining gain values without knowing the CE, which itself depends on antenna gain. Typical values are 2.15dBi for the half-wavelength dipole antenna and 2.55dBi for the one-wavelength [41].

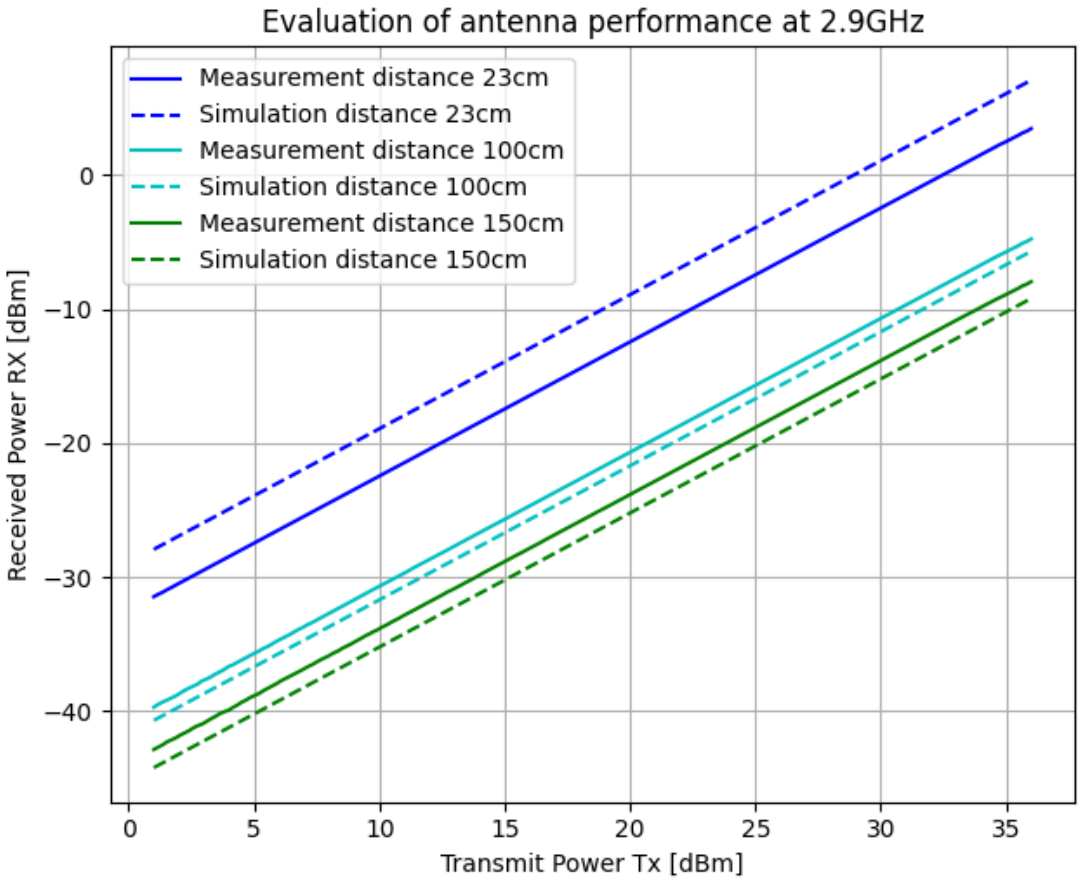

Figure 5.6: The dashed lines are the results expected using the FSPL to predict performance, and the solid curves are the results obtained.

5.3.2 Radiation pattern

Another critical factor to consider is the radiation pattern of our tag, as it remains unknown and significantly impacts system performance due to the dependence of radiated power on the pattern. Since the dipole antenna operates at two frequencies, it will have different radiation patterns: at one frequency, it behaves as a half-wavelength dipole antenna, and at the other, as a full-wavelength dipole antenna. We assume these patterns will resemble those shown in Fig. 5.7

To validate this assumption, VNA measurements were conducted by positioning the tag in the azimuthal plane, with angles α ranging from 0° to 360° in 45° increments, according to the configuration depicted in Fig. 5.8.

With these conditions set, the VNA provided the measurements as detailed in Fig. 5.9.

The antenna does not detect any useful signals with power below -115 dBm. Beyond this threshold, it starts to pick up signals. We also observe that the tag is functioning properly, as there is an increase in performance corresponding to the transmitted power.

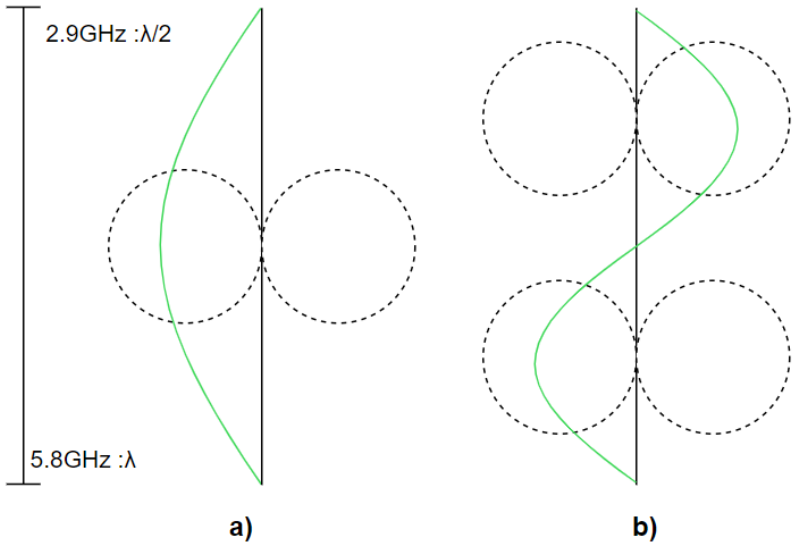

Figure 5.7: Radiation pattern (dashed curves) and current distribution (green curve) in a) half-wavelength dipole and b)one-wavelength dipole

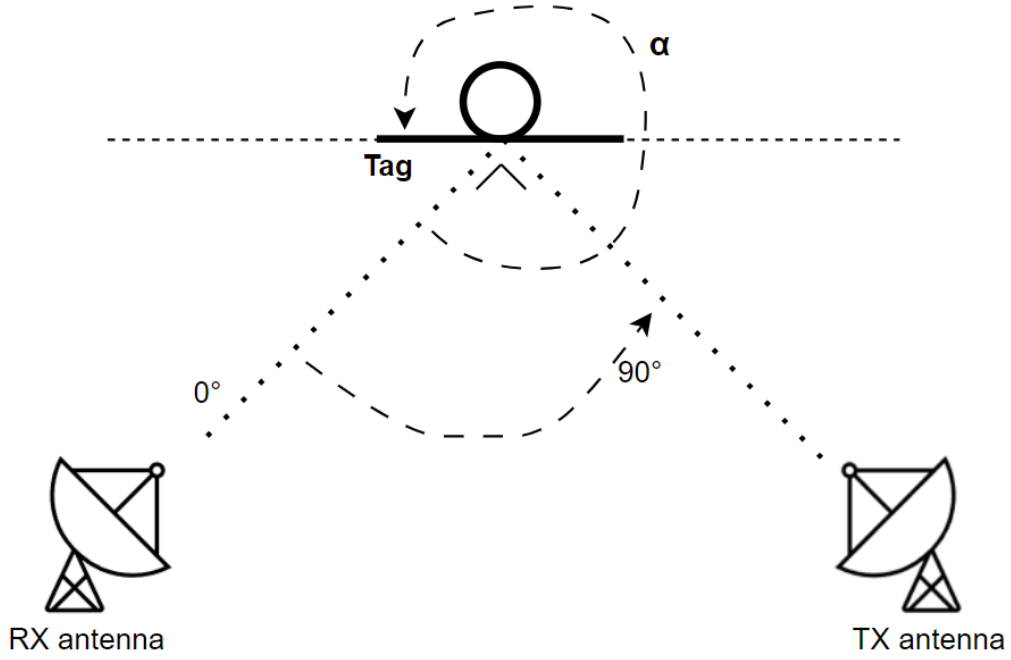

Figure 5.8: Schematic of position of tag for measurement

In this section, you are discussing the observed radiation pattern of the tag as measured during an experiment where the received signal is recorded at various angles, plotted on a polar graph. Fig. 5.10 illustrates the perfromance for different distances.

You note that the observed radiation pattern deviates from the expected theoretical pattern, particularly in the fact that the radiation is not zero at angles like

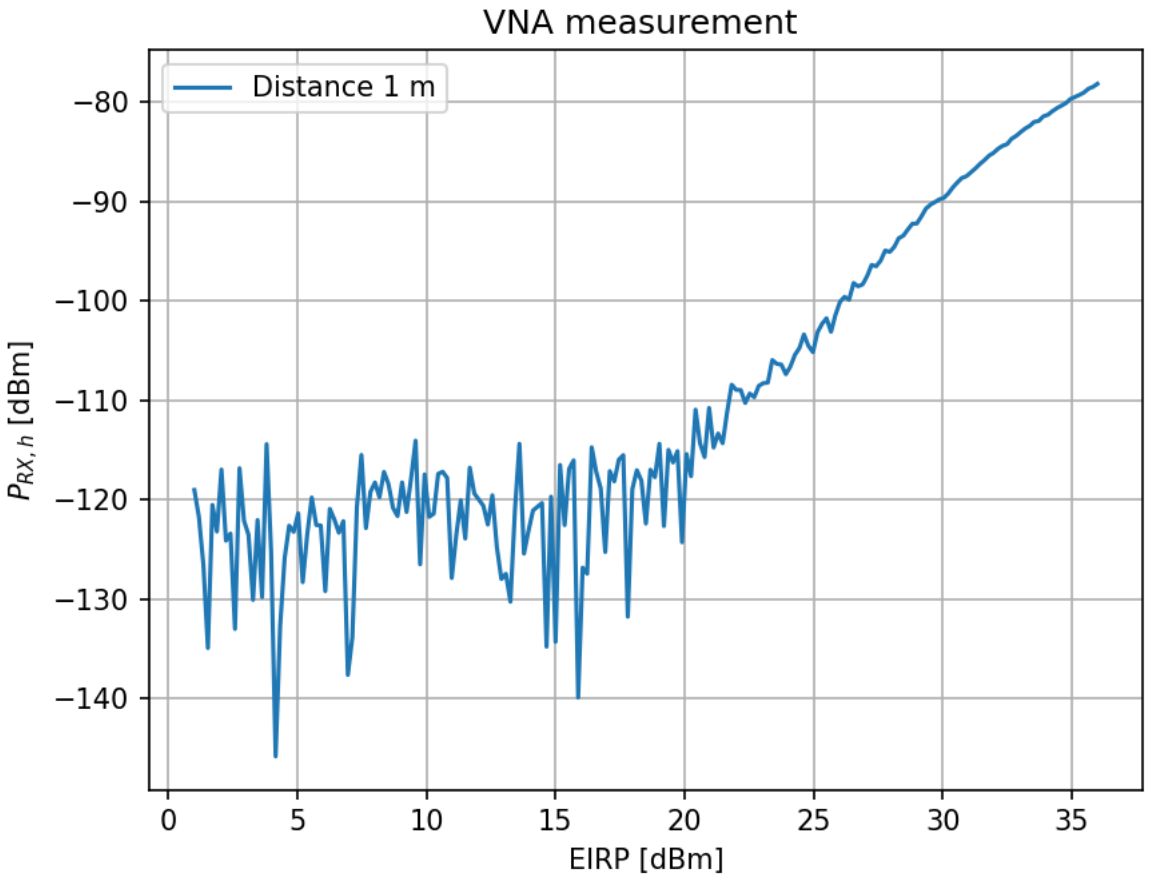

Figure 5.9: Measurement of of performance with angle 315° at distance of 1m with Diode 7630

0° and 90°, where theoretically there should be nulls (no reception).

This discrepancy is attributed to the physical structure of the system, specifically the loop that is part of the tag's design. The presence of this loop likely disrupts the symmetry of the radiation pattern, resulting in non-zero readings at angles where none were expected.

Despite this non-ideal performance, the data still offers valuable insights into the general trends of the tag's radiation characteristics. These insights are useful for understanding the behavior of the tag.

5.3.3 Interpretation

A first insight is the comparison of diode performance based on polar plots to determine which one best suits our application. Observing Fig. 5.11, it appears that the tag equipped with the 7630 diode offers better performance across the various measured angles.

Furthermore, through the verifications performed earlier, we can estimate the CE. By applying the necessary operations to perform reverse engineering on Fig. 5.9

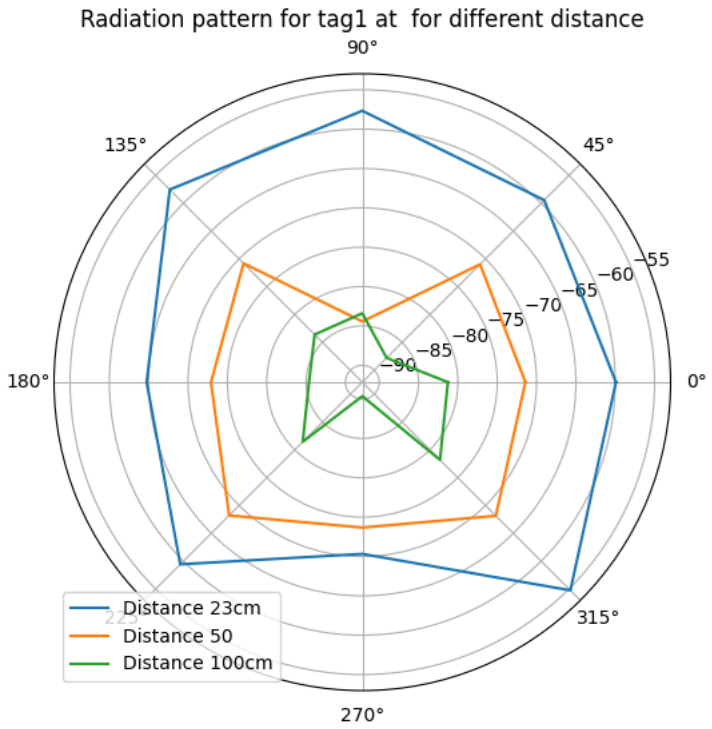

Figure 5.10: Measurement for tag with Diode 7630 by varying distance and angle

and comparing it with the expected performance, we obtain the results illustrated in Fig. 5.12.

One initial observation is that, since we are using measurements from the receiving antenna, readings below 70dB, which represent noise, do not accurately reflect the tag's performance. Additionally, we note similarities with the simulation, though there is a shift along both the vertical and horizontal axes. This can be explained by the fact that the curve represents measurements that would be obtained under the assumption that the radiation pattern is at its full potential, meaning that the tag antenna gain is at its maximum. Since this is not the case here, the antenna gains are lower than those described in the assumptions. As a result, we would need to apply a horizontal translation of the blue curve to the right using 5.1 and a vertical translation using 5.2. However, since the antenna gains are unknown, we cannot perform this adjustment. Nevertheless, the overall trend behavior is consistent with expectations. These observations are more pronounced in Fig. 5.13, which shows measurements taken at a distance of 13cm.

We can observe that the curves are remarkably similar, differing only by a horizontal shift. One factor contributing to this shift is the assumption regarding distance-related losses, which may no longer hold true. Another contributing factor is the assumption about the tag antenna gain mentioned earlier.

Next, we transpose the obtained results into the link budget to examine the differences in performance within our application, as shown in Fig. 5.14.
The causes of these differences can be attributed to several factors, with the associated errors described as follows:

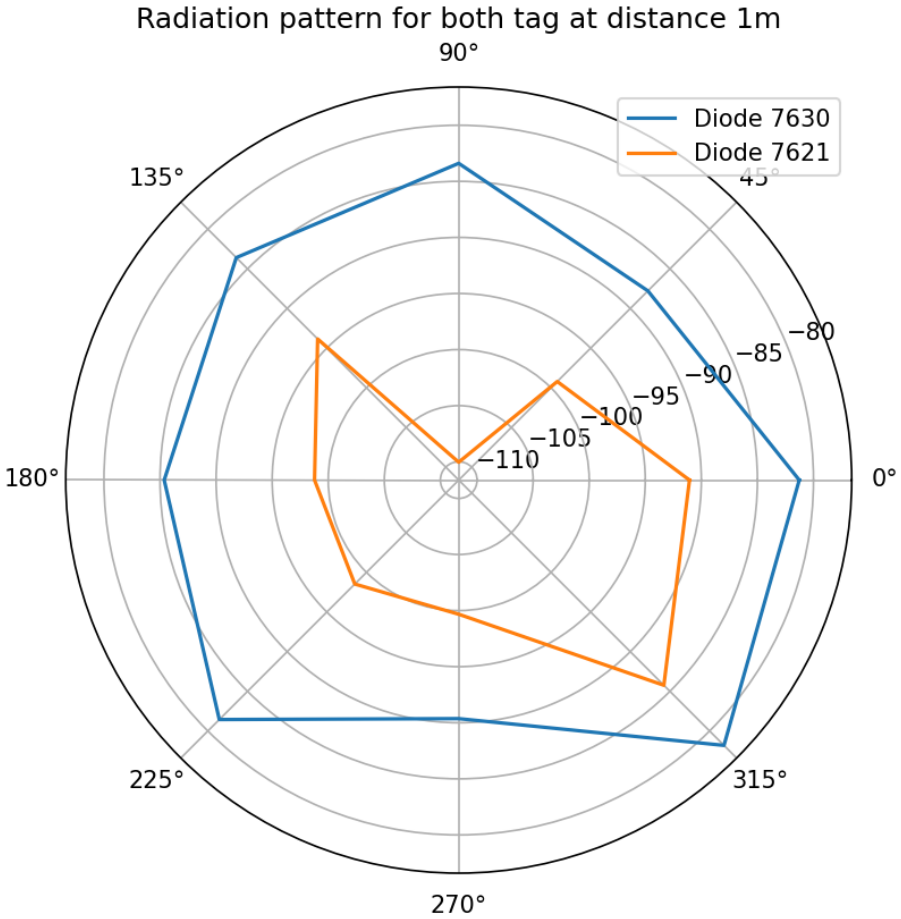

Figure 5.11: Comparison of performance of the different tag at a distance of 1m

- Antenna TagRX Gain : ≈ 0-2.15dB
- Antenna TagTX Gain : ≈ 0-2.55dB
- Difference between inductance used in simulation and reality : ≈ 1dB
- Model of the selected path loss : ≈ 0.5dB

A first comparison can be made with the document [30] where a dipole antenna configuration was also implemented. Since the conversion efficiency varies with the incident power, they generally report values within the range of 0.3-0.9%, corresponding to losses of [-20.4 dB:-25.3 dB]. For an incident power of 6 dBm, a conversion efficiency of 0.8% was recorded, corresponding to a loss of -21dB. Unfortunately, Fig. 5.12 does not include measurements for incident power above 4dBm. However, by combining this with the trend observed in Fig. 5.14, we can assume that extrapolating to a -22dBm output power is feasible, which aligns reasonably well with the literature.We can also consider whether the frequency of the incident signal might impact the conversion efficiency. An initial intuition would suggest that higher frequencies could result in lower conversion efficiency. If our design exhibits similar performance, this implies there is room for improvement.

In the document [6], using the same configuration and frequency as the previous paper, a performance of -16dBm is achieved. The main difference between

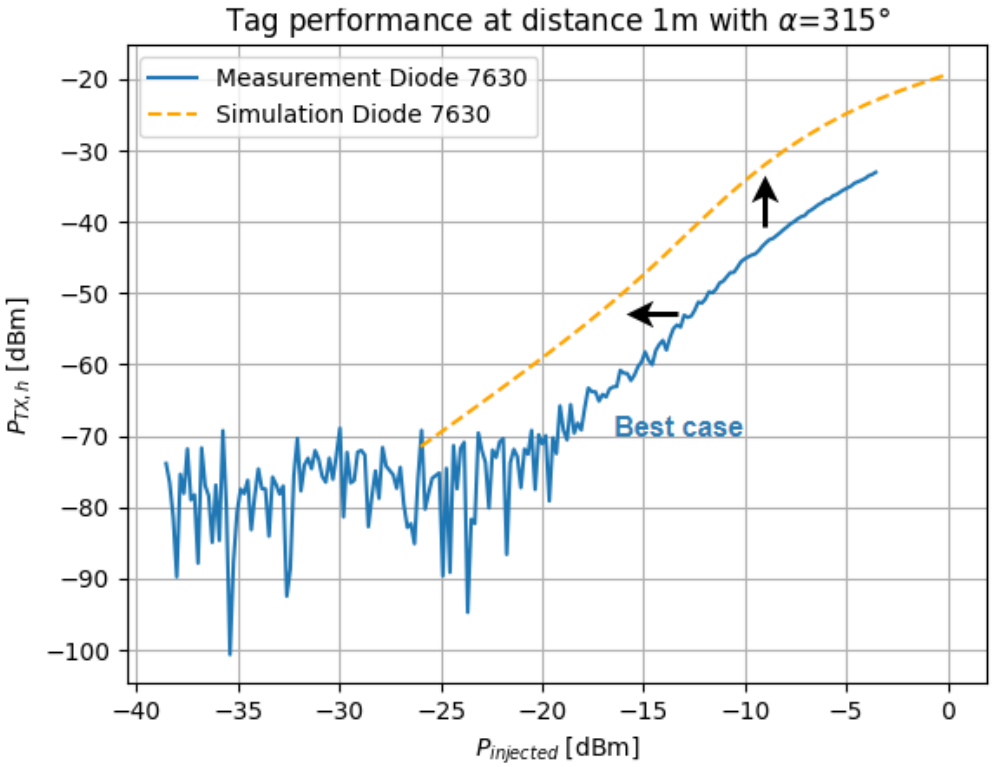

Figure 5.12: Comparison of simulated and measured curves in far field

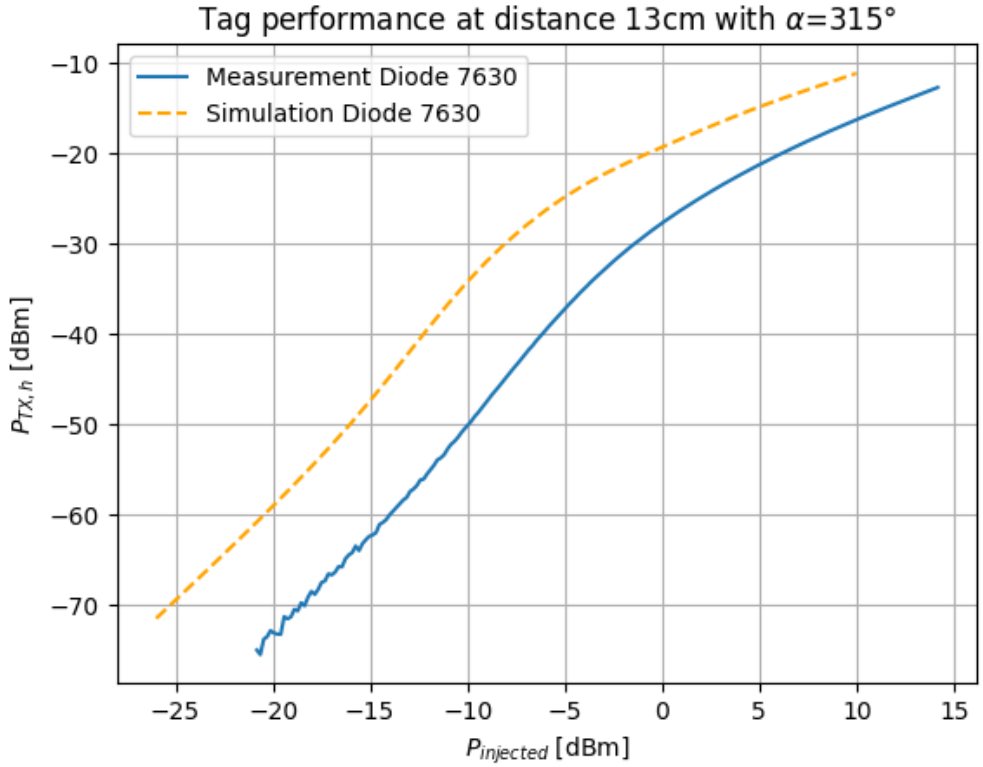

Figure 5.13: Comparison of simulated and measured curves in near field

the two tags lies in the fabrication method: the one used in the previous paper involves constructing the transponder on a miniature glass tube 1mm long, which acts

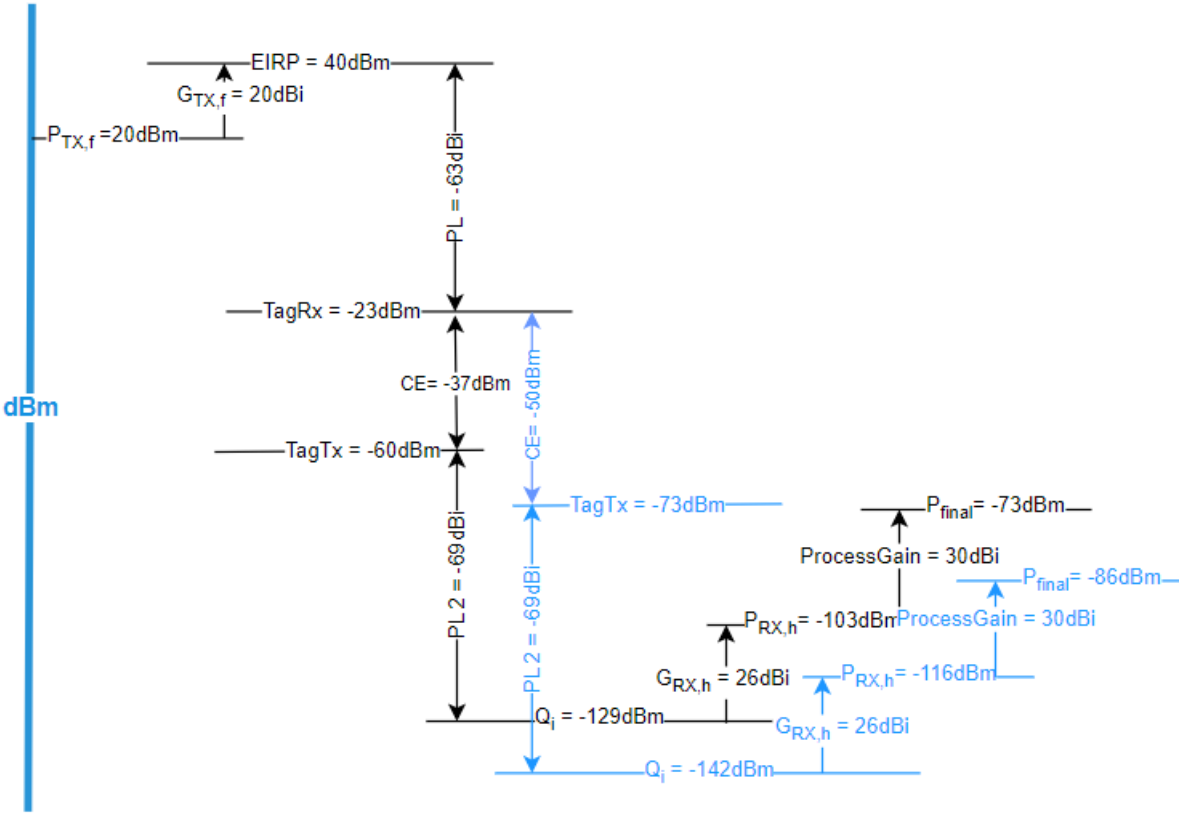

Figure 5.14: Blue line represents performance obtained by measurement and the dark line are from simulation for a distance of 12m

as an electrically insulating central support, while the other is built on a copper wire.

After this comparison, we observe that our design could achieve better performance because it closely resembles the first configuration. By optimizing the antenna placement to maximize directivity during the testig phase , we could potentially reach even better results.

Another point to highlight is that, in the literature [10], it is generally concluded that the SMS7621 diode offers better performance compared to the SMS7630 diode. However, this paper shows the opposite result. This difference can be explained by the fact that the two tags are designed differently: one is mounted on a PCB, while our design uses a dipole antenna. We can therefore conclude that the design has a significant impact on the behavior of the diode.

Chapter 6

Conclusion

The work begins with an overview of the Asian hornet's lifecycle to understand their seasonal activity, allowing us to determine the most appropriate times for intervention. Next, the species' diet is discussed to assess its impact on local ecosystems, particularly on bee populations. To address this threat, a comprehensive review of available technologies in the state of the art is conducted. A criteria-based evaluation table is used to assess and select the most suitable technology for our purposes. Ultimately, the harmonic radar is chosen for its high potential.

The working principle of the system is then explained, starting with the basic theoretical elements of radar operation. Following this, various parameter choices for the system are presented, along with an analysis of the system's performance based on these parameters to predict the maximum detection range. With the selected parameters, predictions indicate that the system remains functional up to a distance of 12 meters. However, to improve this performance, we decided to focus on enhancing a specific component of the system: the tag.

In the process of optimizing tag performance, extensive research on the literature surrounding the choice of diode and configuration is conducted. Following this, the system's best possible performance is analyzed using the selected diodes. Subsequently, a dipole antenna configuration is modeled in ADS, yielding performance results that are 15 dB higher than those reported in the literature.

Finally, an antenna experiment is conducted to validate the simulations. Specific hypotheses are proposed and tested through measurements. However, some uncertainties within the system remain, preventing a fully quantitative interpretation of the results. Nonetheless, the observed trends align well with the simulations, allowing us to conclude that ADS accurately simulates the behavior of various electronic components in a manner consistent with observed trends.

Acknowledgement

First, I would like to express my sincere gratitude to my Master's thesis supervisors, Prof. D. Bol and Prof. D. Lederer, for their unwavering support throughout the year. Their valuable expertise and encouraging words during our bi-weekly meetings enabled me to overcome the major challenges of this thesis.

Second, I am particularly grateful to Prof. C. Craeye for providing the Matlab code to simulate the impedance of the dipole antenna and for his insightful course on antennas and propagation, which closely relates to this work.

Third, I extend my thanks to the members of the ECS group, Marco Gonzalez and Pol Maistriaux, for their constant availability to answer my technical questions.

Fourth, I would also like to express my appreciation to Théo Denis and Arthur Vandroogenbroek. Théo assisted me in navigating ADS, a tool with which I was initially unfamiliar, and provided valuable feedback. Arthur supported me during the laboratory measurements.

I would also like to mention the use of ChatGPT to help me rephrase sentences in this thesis. This tool has helped improve the clarity and fluidity of my writing.

Finally, I am deeply thankful to my familiy and friends for their unwavering support and encouragement.

Bibliography

[1] Aigondigné. *Frelons asiatiques : piéger ou ne pas piéger ?* URL: https://www.aigondigne.fr/mon-cadre-de-vie/environnement/frelons-asiatiques-pieger-ou-ne-pas-pieger/.

[2] Saleh Aljaser. *Miniaturization of a Low Power Harmonic Radar for UAV use.* eng. Student Paper. 2019.

[3] *Antenne radioélectrique.* URL: https://fr.wikipedia.org/wiki/Antenne_radio%C3%A9lectrique#:~:text=Tr%C3%A8s%20grossi%C3%A8rement%20on%20peut%20dire,son%20lobe%20principal%20plus%20%C3%A9troit.

[4] Herbert Aumann et al. "A low-cost harmonic radar for tracking very small tagged amphibians". In: (2013), pp. 234–237. DOI: 10.1109/I2MTC.2013.6555415.

[5] G.L. Charvat, E.J. Rothwell, and L.C. Kempel. "Harmonic radar tag measurement and characterization". In: 2 (2003), 696–699 vol.2. DOI: 10.1109/APS.2003.1219331.

[6] B.G. Colpitts and G. Boiteau. *Harmonic radar transceiver design: miniature tags for insect tracking.* Vol. 52. 11. 2004, pp. 2825–2832. DOI: 10.1109/TAP.2004.835166.

[7] Journal officiel des Communautés européennes. "RECOMMANDATION DU CONSEIL du 12 juillet 1999 relative à la limitation de l'exposition du public aux champs électromagnétiques (de 0 Hz à 300 GHz)". In: *Artificial Intelligence* (1999), pp. 65–67.

[8] DesignSoftTINA. *THÉORÈME DE TRANSFERT DE PUISSANCE MAXIMUM.* URL: https://www.tina.com/fr/maximum-power-transfer-theorem/.

[9] Groupe F. *Le cycle biologique de Vespa Velutina Nigrithorax.*

[10] Xiaoqiang Gu et al. "Readout Distance Enhancement of Battery-Free Harmonic Transponder". In: *IEEE Transactions on Microwave Theory and Techniques* 69.7 (2021), pp. 3413–3424. DOI: 10.1109/TMTT.2021.3068291.

[11] *Institut belge des services postaux et des télécommunications.* URL: https://www.ibpt.be/operateurs/l-ibpt.

[12] Polytech Instrumentation. *VNA.* URL: https://jeulin.com/polytech_fr/polytech/hyperfrequence/vna.html#:~:text=Le%20VNA%20permet%20entre%20autres,ou%20la%20localisation%20de%20d%C3%A9faut.

[13] *ITU.* URL: https://www.itu.int/rec/R-REC-P.676-11-201609-S/en.

[14] Peter Kennedy et al. “Searching for nests of the invasive Asian hornet (Vespa velutina) using radio telemetry”. In: *Communications biology* 1 (July 2018). DOI: 10.1038/s42003-018-0092-9.

[15] Bosung Kim et al. *A Multi-Antenna-based Active Tracking System for Localization of Invasive Hornet Vespa velutina*. 2022, pp. 1693–1697. DOI: 10.23919/ICCAS55662.2022.10003757.

[16] Seungwon Kim et al. *A Tracking Method for the Invasive Asian Hornet: A Brief Review and Experiments*. Vol. 7. 2019, pp. 176998–177008. DOI: 10.1109/ACCESS.2019.2958153.

[17] Nathalie Kleczinski. *Quel est le meilleur appât, la « recette ultime » pour piéger le frelon asiatique ?* URL: https://www.neozone.org/astuces/quel-est-le-meilleur-appat-la-recette-ultime-pour-pieger-le-frelon-asiatique/.

[18] Arjun Kumar and Anastasia Lavrenko. *Compact Folded Meander-Line Harmonic Tag Antenna for Insect Tracking*. 2023, pp. 1–5. DOI: 10.23919/EuCAP57121.2023.10133399.

[19] Anastasia Lavrenko et al. “Design and Evaluation of a Compact Harmonic Transponder for Insect Tracking”. In: *IEEE Microwave and Wireless Components Letters* 30.4 (2020), pp. 445–448. DOI: 10.1109/LMWC.2020.2972744.

[20] *Les champs électromagnétiques et la santé*. URL: http://environnement.wallonie.be/legis/pe/pe009.htm.

[21] Etienne LGF. *Traceur de frelons - LE RETOUR*. URL: https://www.youtube.com/watch?v=mGBM7xquc00&list=RDCMUCzJ7FV2xaYRMUzEuJ9B4dRA&start_radio=1&ab_channel=EtienneLGF.

[22] Rita Abad Lima, Ashish Mishra, and Changzhi Li. *Advantages of Utilizing Higher-order Response for a Harmonic Radar*. 2022, pp. 29–31. DOI: 10.1109/WiSNet53095.2022.9721360.

[23] Riccardo Maggiora et al. “An Innovative Harmonic Radar to Track Flying Insects: the Case of Vespa velutina”. In: *Scientific Reports* 9 (Aug. 2019). DOI: 10.1038/s41598-019-48511-8.

[24] Daniele Milanesio et al. “Design of an harmonic radar for the tracking of the Asian yellow-legged hornet”. In: *Ecology and Evolution* 6 (Feb. 2016), n/a–n/a. DOI: 10.1002/ece3.2011.

[25] Anne Poncelet. “Septembre, le mois de tous les dangers pour les abeilles... et celui de la traque aux frelons asiatiques”. In: *RTBF* (2023). URL: https://www.rtbf.be/article/septembre-le-mois-de-tous-les-dangers-pour-les-abeilles-et-de-la-traque-aux-frelons-asiatiques-11243361.

[26] Jade Prode. *Accueil*. URL: https://www.jabeprode.fr/fr.

[27] Dimitris Psychoudakis et al. “A Portable Low-Power Harmonic Radar System and Conformal Tag for Insect Tracking”. In: *IEEE Antennas and Wireless Propagation Letters* 7 (2008), pp. 444–447. DOI: 10.1109/LAWP.2008.2004512.

[28] Behzad Razavi. *RF Microelectronics (2nd Edition) (Prentice Hall Communications Engineering and Emerging Technologies Series)*. 2nd. USA: Prentice Hall Press, 2011. ISBN: 0137134738.

[29] *Régime alimentaire VVN en provenance du groupe F (lutte contre le frelon asiatique à Bruxelles)*.

[30] J.R Riley and A.D Smith. "Design considerations for harmonic radar to investigate the flight of insects at low altitude". In: *Computers and Electronics in Agriculture* 35 (Aug. 2002), pp. 151–169. DOI: 10.1016/S0168-1699(02)00016-9.

[31] Quentin Rome et al. "Not just honeybees: predatory habits of Vespa velutina (Hymenoptera: Vespidae) in France View supplementary material Not just honeybees: predatory habits of Vespa velutina (Hymenoptera: Vespidae) in France". In: *Annales- Societe Entomologique de France* 57 (Feb. 2021). DOI: 10.1080/00379271.2020.1867005.

[32] Tooba Shams and Pascal Desbarats. *Detection of asian hornet's nest on drone acquired FLIR and color images using deep learning methods*. 2020, pp. 1–6. DOI: 10.1109/IPTA50016.2020.9286693.

[33] Michael Smith, Michael Livingstone, and Richard Comont. "A method for low-cost, low-impact insect tracking using retroreflective tags". In: (Sept. 2021). DOI: 10.32942/osf.io/8bpjh.

[34] SRAWE. *Protéger nos ruches contre le frelon asiatique*. URL: https://www.srawe.be/?page_id=8068#:~:text=Les%20museli%C3%A8res%20tiennent%20les%20frelons,butinage%20proche%20de%20la%20normale..

[35] Greg Storz and Anastasia Lavrenko. *Compact Low-cost FMCW Harmonic Radar for Short Range Insect Tracking*. 2020, pp. 642–647. DOI: 10.1109/RADAR42522.2020.9114612.

[36] Ferry Susanto et al. *Addressing RFID Misreadings to Better Infer Bee Hive Activity*. Vol. 6. 2018, pp. 31935–31949. DOI: 10.1109/ACCESS.2018.2844181.

[37] Nazifa Tahir and Graham Brooker. "Recent developments and recommendations for improving harmonic radar tracking systems". In: (2011), pp. 1531–1535.

[38] Asian Hornet Action Team. *Lifecycle*. URL: https://www.ahat.org.uk/lifecycle.

[39] Agilent Technologies. *Guide to Harmonic Balance Simulation in ADS*. URL: https://edadownload.software.keysight.com/eedl/ads/2011_01/pdf/adshbapp.pdf.

[40] Tom Vrancken (groupe des Vespawatchers). *Méthode de localisation des nids de frelons asiatiques*. 2023.

[41] Wikipédia. *Antenne dipolaire*. URL: https://fr.wikipedia.org/wiki/Antenne_dipolaire.

[42] Wikipédia. *Vespa velutina*. URL: https://fr.wikipedia.org/wiki/Vespa_velutina.

[43] Wikipedia. *Near and far field*. URL: https://en.wikipedia.org/wiki/Near_and_far_field.

[44] Wikipedia. *Radio-identification*. URL: https://fr.wikipedia.org/wiki/Radio-identification.

[45] Glenlivet Wildlife. *Asian Hornet (Vespa Velutina)*. URL: https://glenlivet-wildlife.co.uk/insects/asian-hornet/.

UNIVERSITÉ CATHOLIQUE DE LOUVAIN
École polytechnique de Louvain
Rue Archimède, 1 bte L6.11.01, 1348 Louvain-la-Neuve, Belgique | **www.uclouvain.be/epl**